ADVANCED FUNCTIONAL MATERIALS
www.afm-journal.de

Muticomponent Melt-Electrowritten Vascular Graft to Mimic and Guide Regeneration of Small Diameter Blood Vessels

*Angelica S. Federici, Orquidea Garcia, Daniel J. Kelly, and David A. Hoey**

Cardiovascular disease is a leading cause of morbidity. Current treatments include vessel substitution using autologous/synthetic vascular grafts, but these commonly fail in small diameter applications, largely due to compliance mismatch and clot formation. In this study, a multicomponent vascular graft, that takes inspiration from native vessel architecture, is developed to overcome these limitations. Melt electrowriting (MEW) is used to produce tubular scaffolds with vascular-mimetic fiber architecture and mechanics, which is combined with a lyophilized fibrinogen matrix with tailored degradation kinetics to generate a hybrid graft. The MEW framework not only contributes to graft mechanics, but also provides contact guidance to direct cell/neotissue orientation and mimic the native tunica media. This construct is further functionalized with heparin, which in combination with the smooth extracellular matrix (ECM) surface, reduced platelet adhesion and clot formation providing a substrate for endothelization, thereby mimicking the function of the intima. Lastly, an outer electrospun layer representing the adventitia is added to improve elasticity and reduce permeability. This graft satisfies ISO implantability requirements, matches the compliance of native vessels, and reestablishes physiological flow with minimal clot formation in a preclinical model. Therefore, this graft represents an innovative off-the-shelf alternative to address the unmet clinical need for small-diameter vascular grafts.

1. Introduction

Cardiovascular disease (CVD) is recognized as one of the leading causes of mortality worldwide,[1–3] with estimated medical costs expected to reach over one trillion dollars by 2035. Coronary heart disease (CHD) and peripheral vascular disease (PAD) are the most common presentations, with CHD affecting between 2% and 6% of the total population. In advanced stages of these diseases, where there is an occlusion of the whole lumen, a total vessel substitution is required[4] and a ready-to-use graft is essential.[5] Autograft implantation is the current gold standard for vascular bypass[6,7] but is limited in both availability and long-term patency.[7–9] Therefore, alternative strategies such as synthetic vascular grafts (SVGs) have emerged. Undeniably, SVGs demonstrate good success for medium to large diameter blood vessel substitution[7] but fail for small diameter blood vessels (<6 mm in diameter) where they do not successfully restore correct blood flow due to restenosis that occurs as a primary consequence of mechanical compliance mismatch and clot formation.[10–12]

To address the limitation of SVGs, recent efforts have focused on degradable tissue engineering vascular grafts (TEVGs) that look to mirror the native composition and architecture of the vessel wall to achieve the mechanical and biological properties required to prevent failure.[13] The native blood vessel wall consists of three concentric layers (tunica intima,

A. S. Federici, D. J. Kelly, D. A. Hoey
Department of Mechanical, Manufacturing and Biomedical Engineering
School of Engineering
Trinity College
Dublin D02PN40, Ireland
E-mail: dahoey@tcd.ie

A. S. Federici, D. J. Kelly, D. A. Hoey
Trinity Centre for Biomedical Engineering
Trinity Biomedical Sciences Institute
Trinity College
Dublin D02R590, Ireland

A. S. Federici, D. J. Kelly, D. A. Hoey
AMBER
The SFI Research Centre for Advanced Materials and Bioengineering Research
Dublin D02W085, Ireland

O. Garcia
Johnson & Johnson 3D Printing Innovation & Customer Solutions
Johnson & Johnson Services, Inc.
Irvine 92618, CA, USA

D. J. Kelly, D. A. Hoey
Department of Anatomy and Regenerative Medicine
Royal College of Surgeons in Ireland (RCSI)
Dublin D02 YN77, Ireland

The ORCID identification number(s) for the author(s) of this article can be found under https://doi.org/10.1002/adfm.202409883

DOI: 10.1002/adfm.202409883

tunica media, and tunica adventitia), each of which possesses a unique ECM composition and structure (fibers oriented ≈18.8°, ≈37.8°, and ≈58.9° from intima to adventitia) which is critical to function.[11,12,14–18] While electrospinning can produce off-the-shelf grafts consisting of synthetic polymeric fibers comparable in size to native ECM, it is limited by the accuracy in fiber deposition and thus is unable to recapitulate the highly organized structure, mechanical properties, and bioactivity of the vessel wall. Alternative approaches involve long term in-vitro cell culture on biomaterial scaffolds or utilization of scaffold free cell sheet technologies to produce more biomimetic grafts.[19] While these grafts represent a significant improvement on current off-the-shelf alternatives, they have a protracted manufacturing process and still fall short of the required mechanical performance.[20–22]

The limitations in current approaches has fueled the development of novel fabrication methods with high accuracy, structural control, and bioactivity.[7,10,11] MEW is one such technology that can produce and accurately deposit fibers in the micron diameter range. MEW is thus capable of creating an environment that mimics the ECM fiber resolution and architecture of native tissues, enabling a closer match to the mechanical and biological properties of native tissues, including bone,[23-26] cartilage,[27] skin,[28] heart valves,[29] and importantly vessels.[18,20,30] For example, our group and others have demonstrated that MEW can recapitulate the blood vessel wall architecture through rhombus or auxetic designs simulating the different features and mechanical properties of each tunica[18,31,32] that act as contact guiding structures to orientate cell and neotissue deposition, and can also be combined with electrospun membranes to support endothelialization.[20,33] However, the high porosity of MEW based scaffolds hinders cell attachment and the use of synthetic polymers fail to recreate a robust environment for tissue regeneration.[34] Therefore, alternative strategies have included the combination of synthetic scaffolds with ECM based hydrogels,[35,36] volumetric bioprinting,[37] or lyophilized ECM scaffolds[38] to better recapitulate the physiological environment that cells sense in vivo.[39,40] With regard to vascular applications, one of the most explored ECMs is fibrin, due to its role in coagulation.[41,42] A hybrid solution combining both synthetic and natural polymers such as fibrinogen can be adopted to compensate for their respective limitations: inducing a positive interaction between cells and scaffolds through the natural ECM components and to maintain excellent mechanical performance through a MEW polymeric framework.[39,43]

Therefore, in this study, we developed a multicomponent off-the-shelf vascular graft, that took inspiration from native vessel architecture, to address the current limitations of synthetic alternatives. Building on our previously developed tubular melt-electrowritten framework with vascular mimetic fiber architecture and mechanics,[18] we combined this structure with a lyophilized fibrinogen matrix with tailored degradation kinetics. This hybrid construct significantly enhances neotissue formation while still enabling the MEW framework to provide contact guidance controlling cell and neotissue orientation, representing the tunica media. This construct was further functionalized with heparin, which in combination with the smooth ECM surface, reduced platelet adhesion and clot formation and provided a substrate for endothelization, representing the tunica intima. Lastly, an outer electrospun layer was added to improve elasticity and reduce permeability, representing the tunica adventitia. This vascular mimetic graft satisfied ISO implantability requirements, matched the compliance of native vessels, and reestablished physiological flow with minimal clot formation in a preclinical model.

2. Results

2.1. Fabrication of a Multicomponent Off-the-Shelf Vascular Graft

A multicomponent MEW vascular graft was successfully fabricated combining three different fabrication technologies in a scalable step-by-step assembly process to recapitulate the three layers of a native vessel (**Figure 1**A,B). MEW PCL tubular frames were fabricated as previously described,[18,44] where fibers were deposited on a rotating mandrel with high accuracy at an angle of 71.6° to mimic the highly organized collagen and elastin architecture of the tunica media (Figure 1Bi,C). Second, within the pores of this frame, a fibrinogen-based lyophilized ECM component was added to increase cell adhesion, infiltration, and bioactivity and provide a tunica intima like lumen to facilitate endothelization (Section 2.1.1) (Figure 1Bii,C). Lastly, an elastic Poly(L-lactide-co-ε-caprolactone) (PLCL) electrospun layer was successfully added to the outer surface of the graft representing the tunica adventitia of native blood vessels (Figure 1Biii,C) (Section 2.1.2). The detailed fabrication and optimization of each layer is discussed below.

2.1.1. Fabrication of the Tunica Media/Intima Region of Vascular Graft

Infusion of a fibrinogen ECM solution into a MEW framework was investigated in terms of solution concentration, freezing temperature, and chemical crosslinking in order to explore the impact on porosity, pore size, and degradation profile of the ECM component (**Figure 2**; Figure S1, Supporting Information). Initially, a fibrinogen solution at concentrations of 20 and 50 mg mL^{-1} were lyophilized at temperatures of −20, −40 and −80 °C, and all successfully formed a porous ECM scaffold (Figure S1A, Supporting Information). Given the soluble nature of fibrinogen, these scaffolds were further cross-linked with GTA (Figure S1B, Supporting Information). Analysis of scaffold gross morphology and porosity (Figure S1B,C, Supporting Information) revealed that the 20 mg mL^{-1} lyophilized ECMs collapsed partially after crosslinking, while the 50 mg mL^{-1} maintained their shape. Moreover, the 50 mg mL^{-1} lyophilized at −80 °C contained a consistent high porosity (Figure S1C, Supporting Information) and thus was brought forward for infusion inside a MEW framework. The samples obtained with a fibrinogen concentration of 50 mg mL^{-1} and a freezing temperature of −80 °C demonstrated excellent infusion and a homogenous ECM structure bound to the MEW framework following lyophilization (Figure 2A,B). These ECM structures were further successfully cross-linked with either EDC/NHS or GTA which represent both a mild and more aggressive cross-linking procedure, respectively. An analysis of scaffold morphology was performed and both treatments resulted in an ECM pore size

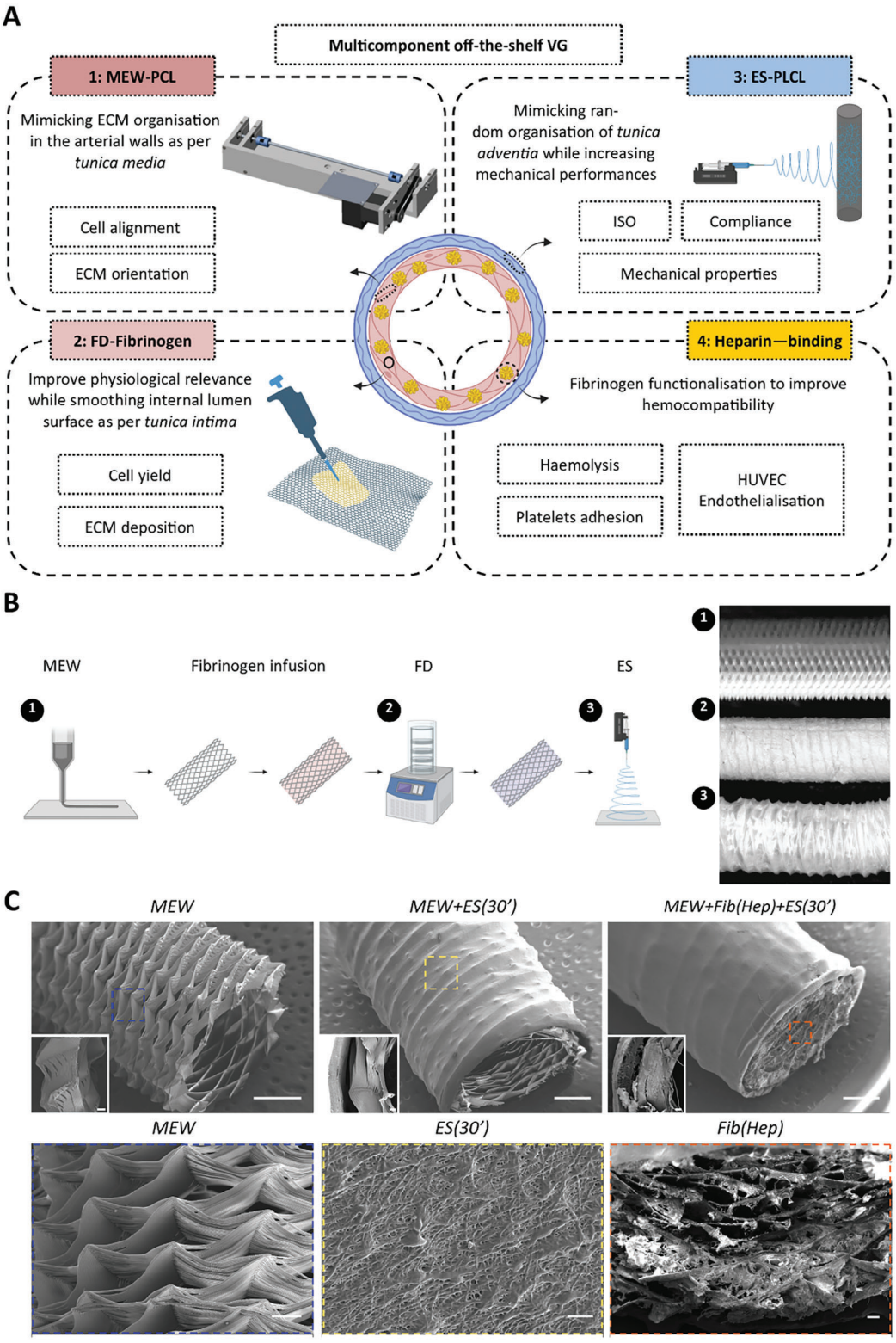

Figure 1. Vascular graft development, step-by-step assembly process, and morphological evaluation. A) Schematic representation of the key components of the proposed vascular graft. B) Schematic representation of development process from MEW to fibrinogen infusion and electrospinning. Step-by-step graft morphological characterization along with further process and layer implementation. C) SEM images of vascular graft. From left to right: MEW frame alone, enclosed in a PLCL electrospun (ES) layer, and MEW infused with a lyophilized crosslinked fibrinogen ECM (Fib) covered on the outside with a PLCL electrospun (ES) layer. Scale bar from top to bottom 1 mm, and 100 µm respectively. Magnified images for MEW frame alone, PLCL electrospun (ES) layer over MEW frame and infused fibrinogen (Fib) sponge into tubular MEW graft. Scale bar 200, 10, and 100 µm, respectively.

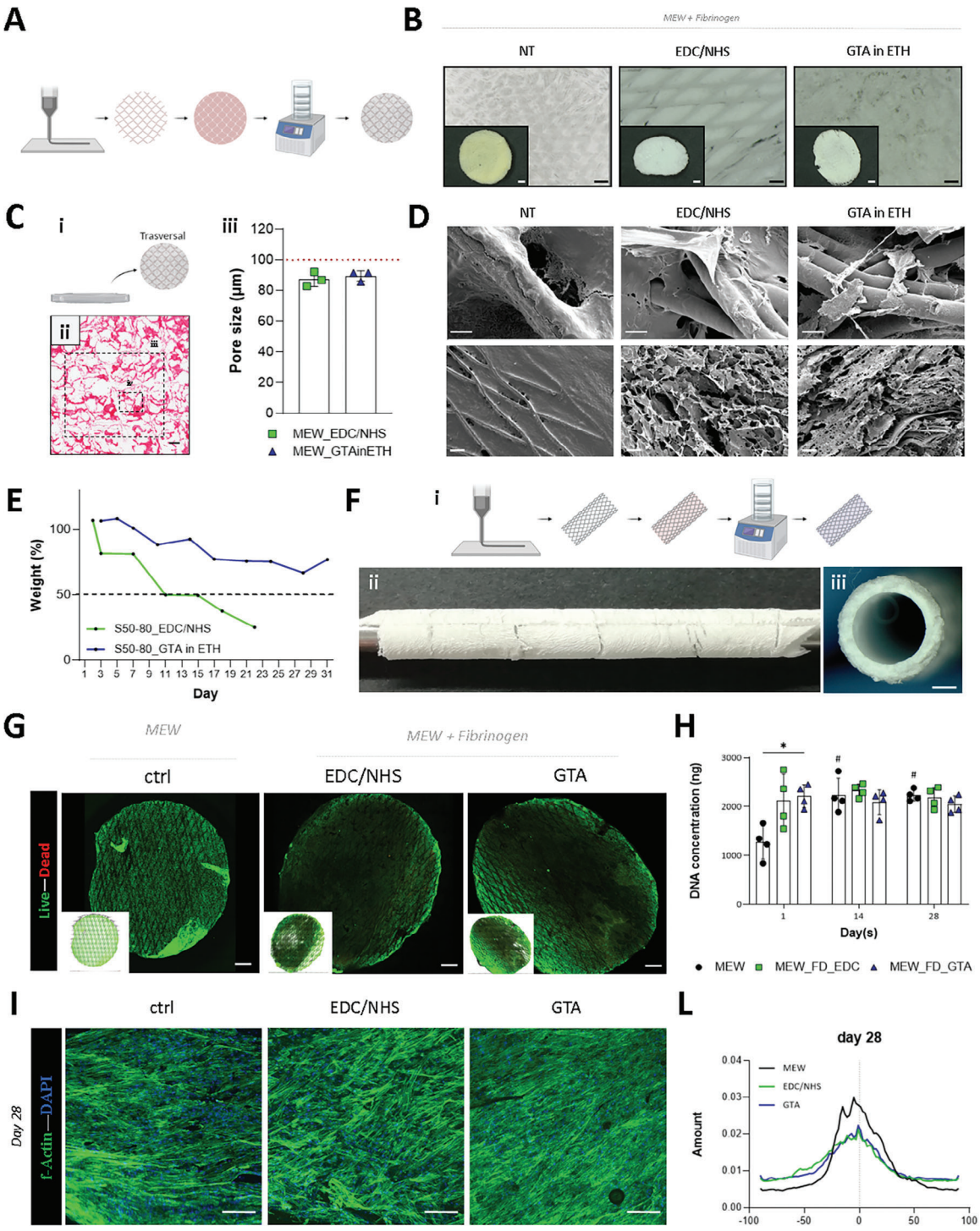

Figure 2. Impact of lyophilized fibrinogen and crosslinking method on cell colonization and orientation. A) Schematic representation of fabrication process from MEW printing to fibrinogen infusion. B) Qualitative morphological evaluation of fibrinogen infusion. Overall sample original magnification 1 x and 5 x, scale bar 1 mm and 200 µm, respectively. C) Pore size analysis of infused and crosslinked MEW+Fib samples. D) SEM images of infused devices crosslinked with EDC/NHS and GTA in comparison with the noncrosslinked control (NT). Original magnification 1.5 kx, 500 x, and 100 x. Scale bar 10 µm, 10 µm, and 100 µm, respectively. E) Degradation profile for the two different crosslinking methods. F) (i) Schematic representation of fabrication process translation from planar to tubular samples with (ii) a representative image of the infused vascular graft overall structure and (iii) the cross-section. Scale bar 1 mm. G) Live dead images representative of each group at day 28. Scale bar 500 µm. H) DNA quantification of MEW alone and MEW+Fib samples in comparison at day 1-14-28. *p* value $^{*}\leq 0.05$, $^{**}\leq 0.005$, $^{***}\leq 0.001$, and $^{****}\leq 0.0001$. Evaluation of single group evolution at different time points identified by # statistically different from day 1. I) Representative images of *F*-actin (green) and DAPI (blue) staining for all the groups at different time points (day 1-14-28). Scale bar 100 µm. L) Directionality analysis of *f*-actin fibers at (i) day 1, (ii) day 14, (iii) day 28. Graph showing the amount of fibers with the same orientation and directionality preference. ($n = 4$, $N = 3$).

≈90 µm, which closely matches the pore size previously reported to be optimal for smooth muscle cell (SMC) infiltration and proliferation[45,46] (Figure 2C,D). Interestingly, samples treated with EDC/NHS and GTA demonstrated significantly different degradation profiles, with a fast degradation reported for EDC/NHS (50% weight loss after 9 days), while the GTA-treated scaffolds maintain greater than 50% weight for the duration of the 31-days analysis (Figure 2E).

The best performing ECM infusion protocol was then translated into a tubular graft; 50 mg mL^{-1} fibrinogen solution was added to NaOH-treated PCL samples and frozen at −80° for a minimum of 1 h before lyophilization for 18 h at 0.2 PSI (Figure 2F). The key design criteria was for a scalable production process with interchangeable rods from the MEW set-up to the infusion device, for a minimum graft length of 5 cm with internal diameter of 3 mm and thickness comparable to the height of the tunica media and MEW printed frameworks (≈600 µm). The device developed here (Figure S2, Supporting Information) ensured ease of manufacture, versatility, and ease of use. Briefly, O-rings were allocated at both extremities of the metal rods and the two components screwed in place after the matching pins secured the right alignment. Fibrinogen solution was infused from the opening on the upper side of the design and demonstrated perfect sealing. The resulting device was able to accommodate three rods of 3 mm diameter with MEW tubular samples of 5 cm in length leaving just the space between pores to be infilled with an ECM (Figure S2, Supporting Information). After freezing, the infused device was separated, and samples left on the rods to lyophilize so that collapsing of the structure could be prevented. Fibrinogen infused tubular samples demonstrated good stability and homogenous pore distribution before and after the crosslinking process (Figure 2F).

2.1.2. Fabrication of the Tunica Adventitia Region of Vascular Graft

A combination of parameters (voltage, flow rate, distance to collector) was evaluated in order to optimize the electrospinning of a 20% PLCL (dissolved in formic and acetic acid at a ratio of 60:40) fibrous layer over a rotating mandrel (Figure S3, Supporting Information). SEM images were utilized to evaluate the quality of the obtained scaffolds. Increasing the voltage resulted in an increase in bead formation and an inhomogeneity of fiber diameter. Increasing the applied flow rate resulted in a more compact mesh with visible formation of fused fiber agglomerates (Figure S3A, Supporting Information). Increasing the distance between the charged needle and the grounded collector resulted in further deterioration of the final scaffold, where fibers were largely absent, and the number of visible defects was intensified (Figure S3B, Supporting Information). Therefore, based on this optimization study, the following parameters were brought forward and used for the last step in the fabrication process: flow rate of 1 mL h^{-1} with a distance of 10 cm and a voltage of 9 kV, which resulted in a homogenous fibrous PLCL membrane. The electrospinning time adopted was 30 min which granted a suitable vascular graft while the 3 h spinning time was considered superfluous in terms of mechanical performance (see Section 2.4). Brightfield and SEM images illustrate the impact of the fibrinogen infusion on the pattern of the PLCL layer on the MEW framework (Figure 1C), whereby electrospinning onto the MEW+Fib hybrid frameworks resulted in a more stable and uniform distribution of PLCL fibers due to the higher surface area, resulting in excellent integration with the other two components making up the tunica media.

2.2. Biological Evaluation

2.2.1. Cell Adhesion, Proliferation, and Alignment

Both the MEW scaffold alone (Ctrl) and MEW+Fib hybrid scaffolds, crosslinked with either EDC/NHC or GTA, were fully colonized with hMSCs within two weeks. Neither crosslinking method affected cell viability at any stage during the 28 days of maturation as clearly visible with the live/dead staining (Figure 2G). A more accurate evaluation of seeding efficiency and cell proliferation was obtained through DNA quantification (Figure 2H). Hybrid MEW-ECM samples demonstrated a significantly higher DNA quantity at day 1, which is the evidence of a higher cell retention during the initial seeding process and represents the impact of the ECM component in capturing cells. This initial difference was not observed by day 14. MEW samples, even when not infused with a fibrinogen scaffold, were able to accommodate cell proliferation resulting in colonization of the whole scaffold, as demonstrated by no difference in DNA content between the Ctrl and both the EDC/NHS and GTA treated samples by day 14 (Figure 2H).

A key feature of the MEW framework is the biomimetic 18.4° fiber winding angle that mimics the collagen fiber organization of the native tunica media.[18] This structure not only recapitulates the mechanical performance of the media but importantly also provides contact guidance to ensure infiltrating cellular alignment along the major diagonal, as previously demonstrated.[18] Importantly, this cellular alignment was not impacted by the infusion of the fibrinogen ECM. *F*-actin staining was performed to better characterize cell alignment over time and how ECM infusion and cross-linking may affect this (Figure 2I). No alignment was observed for samples on day 1. The MEW alone samples (Ctrl) showed two peaks centered ≈18°, which represents the orientation of the MEW PCL framework, thus demonstrating that the first interaction between cells and scaffolds occurs along the PCL fibers in the Ctrl group (Figure 2). These peaks were not observed in the infused samples, indicating that the cells preferentially bound to the fibrinogen ECM. As the cells colonized the MEW frame the alignment increased in all samples, with no major difference between EDC/NHS and GTA treatment at day 14 (Figure S4, Supporting Information). While there remained no difference in alignment between the infused samples at day 28, a more dominant cell alignment was evident in the MEW alone samples (Ctrl) (Figure 2L).

2.2.2. ECM Production and Organization

The presence of lyophilized fibrinogen within the MEW frame increased the overall production of ECM, and the shorter degradation time of the EDC/NHS crosslinked samples enabled the PCL frame to preferentially orientate the newly deposited ECM along the major diagonal (**Figure 3**). Histological sections of

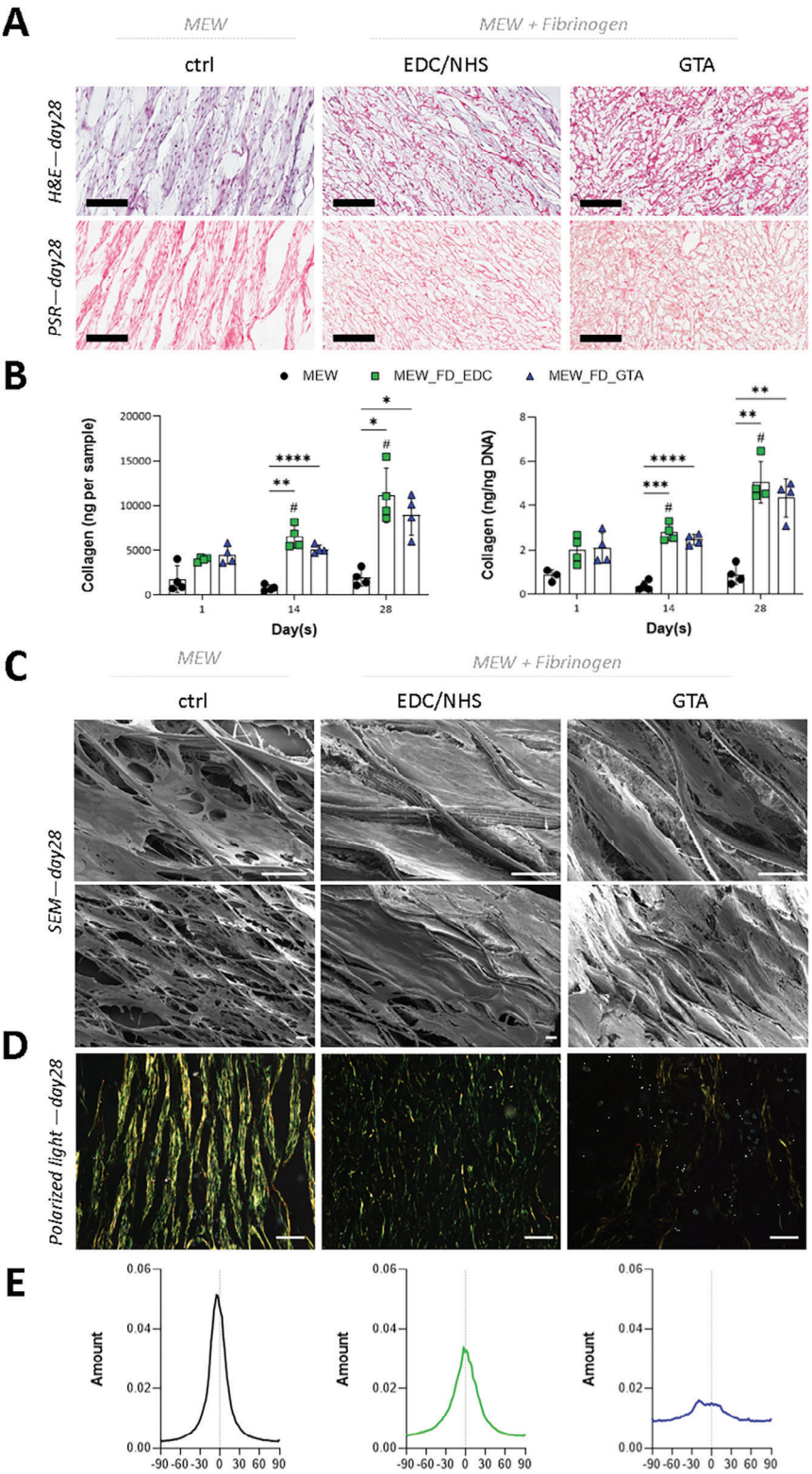

Figure 3. ECM deposition and orientation analysis. A) Histological staining of samples at day 28 with H&E staining and Picrosirius Red staining. Original magnification 10 X, Scale bar 200 µm. B) Collagen content for all the groups in comparison at day 1-14-28 as ng per samples and normalized for the respective content of DNA. *p* value $^{*}\leq 0.05$, $^{**}\leq 0.005$, $^{***}\leq 0.001$, and $^{****}\leq 0.0001$. Evaluation of single group evolution at different time points identified by # statistically different from day 1, & statistically different from day 14. C) SEM images for all the groups cultured for 28 days. Scale bar 20 µm and 100 µm, respectively. D) Polarized light images for all the groups cultured for 28 days. Scale bar 200 µm. E) Directionality analysis of collagen fibers. Graph showing the number of fibers with the same orientation and directionality preference.

Table 1. Schematic representation of different heparinization processes divided per steps.

		Pretreated sample	Crosslinking 1 in ethanol	Crosslinking 2 in MES
1-step	(a)	Fibrinogen	EDC/NHS	N/A
	(b)	Fibrinogen	EDC/NHS + heparin	N/A
	(c)	Fibrinogen + heparin	EDC/NHS	N/A
2-steps	(a)	Fibrinogen	EDC/NHS	EDC/NHS + heparin
	(b)	Fibrinogen	EDC/NHS	EDC/NHS + heparin + laponite

samples at day 28 were stained with H&E and picrosirius red (PSR) to visualize cell organization and ECM production respectively, with particular attention paid to collagen deposition (PSR) as it is the main component of the vessel wall (Figure 3A). H&E staining demonstrated a highly cellularized tissue in each construct. PSR staining indicated that this tissue consisted of collagen, and there was evidence of an alignment of this ECM in the Ctrl and to a smaller extent, in the EDC/NHS treated samples. A more random distribution of collagen was observed in GTA-treated MEW+Fib constructs (Figure 3A). Upon quantification of collagen deposition through hydroxyproline, it was found that collagen deposition increases with time, and that there was a significant enhancement in collagen deposition in the MEW+Fib hybrid scaffolds, crosslinked with either EDC/NHS or GTA, when compared to the MEW scaffolds alone, both in terms of total collagen and collagen produced per cell (Figure 3B).

Further analyses were performed to better understand ECM organization, as this represents an important property in the long-term survival of vascular grafts. SEM images of all groups at day 28 highlighted the full infilling of MEW pores with a dense tissue evident in all groups (Figure 3C). Specifically, MEW samples (Ctrl) alone and EDC/NHS treated hybrid samples demonstrated good cell infusion, ECM deposition and orientation, while in the GTA-treated MEW+Fib samples, the fibrinogen infused ECM was still visible below the upper cell sheet (Figure 3C). This trend was further identified through polarized light microscopy and analysis (Figure 3D). Quantitative data of collagen fiber directionality demonstrated a higher orientation for MEW alone (Ctrl) samples and EDC/NHS hybrid samples compared to the GTA treated group (Figure 3E). Indeed, the GTA-treated hybrid scaffold showed almost no alignment of collagen fibers at day 28, indicating that the fibrinogen ECM is shielding the cells and neo-tissue from the contact guidance provided by the MEW framework. The preferential direction of collagen fiber deposition along the major diagonal of MEW alone and fast degrading EDC/NHS-treated MEW+Fib samples recapitulates the collagen organization seen in native tissue vessels, where it preferentially aligns in the circumferential direction.

Thus, based on initial cell adhesion, ECM deposition and orientation, the EDC/NHS crosslinking treatment was brought forward for all subsequent studies.

2.3. Heparin Functionalization

A stable heparin binding to the fibrinogen infused ECM was successfully achieved to improve hemocompatibility (**Figure 4**). The crosslinking solution of EDC/NHS that has previously demonstrated to be effective in stabilizing fibrinogen scaffolds, was enriched with heparin following an optimization process (Figure 4A and **Table 1**). Specifically, in Figure S5A (Supporting Information) Toluidine Blue (TB) color variation was adopted to verify heparin binding, thanks to the specific binding of TB to chemical modified sulfonic groups. A strong intensity of heparin binding was reported for scaffold crosslinked first in ethanol with EDC/NHS and further stabilized in MES buffer enriched with heparin. Moreover, TB was adopted to quantify the cumulative release of heparin over 10 days (Figure S5B, Supporting Information). A plateau was reached within 24 h for all samples that underwent 1-step crosslinking indicating an instability of these binding procedures. On the contrary, prolonged and controlled release was achieved with the 2-step crosslink method – (Fib-EDC/NHS)Hep.

2.3.1. Hemocompatibility Assessment

The established anticoagulant properties of heparin reduced the hemolytic behavior and platelet adhesion, overall improving the interaction between blood and the developed graft. Hemolysis quantification was performed by reading supernatant absorbance after 1 h incubation with whole blood at 37 °C. Non-hemolytic behavior was detected in all groups, with an average rate lower than 1% (Figure 4B,C). Furthermore, the number of adherent platelets was calculated using SEM images for the 2-step crosslink method (Table 1-2-steps) samples after 2 h incubation with PRP (Figure 4D,F). The results highlighted the capacity of integrated heparin to significantly reduce the overall number of adhered platelets compared to unfunctionalized control grafts (Fib-EDC/NHS). No significant difference was identified between functionalized groups, although larger variability was evident in the laponite containing samples (Figure 4F).

Therefore, with the information gathered with these tests, a primary crosslink with EDC/NHS and a second crosslinking process in MES enriched with heparin, demonstrated higher stability and gradual release of heparin over 10 days. Moreover, blood interaction with this procedure was enhanced with a reduced hemolytic effect and adherent platelet number. This method was thus utilized in all future studies.

2.3.2. Endothelialization

Heparin enriched MEW+Fib(Hep) vascular grafts demonstrated good interaction with endothelial cells and enhanced capacity for endothelium formation (Figure 4G). HUVECs were

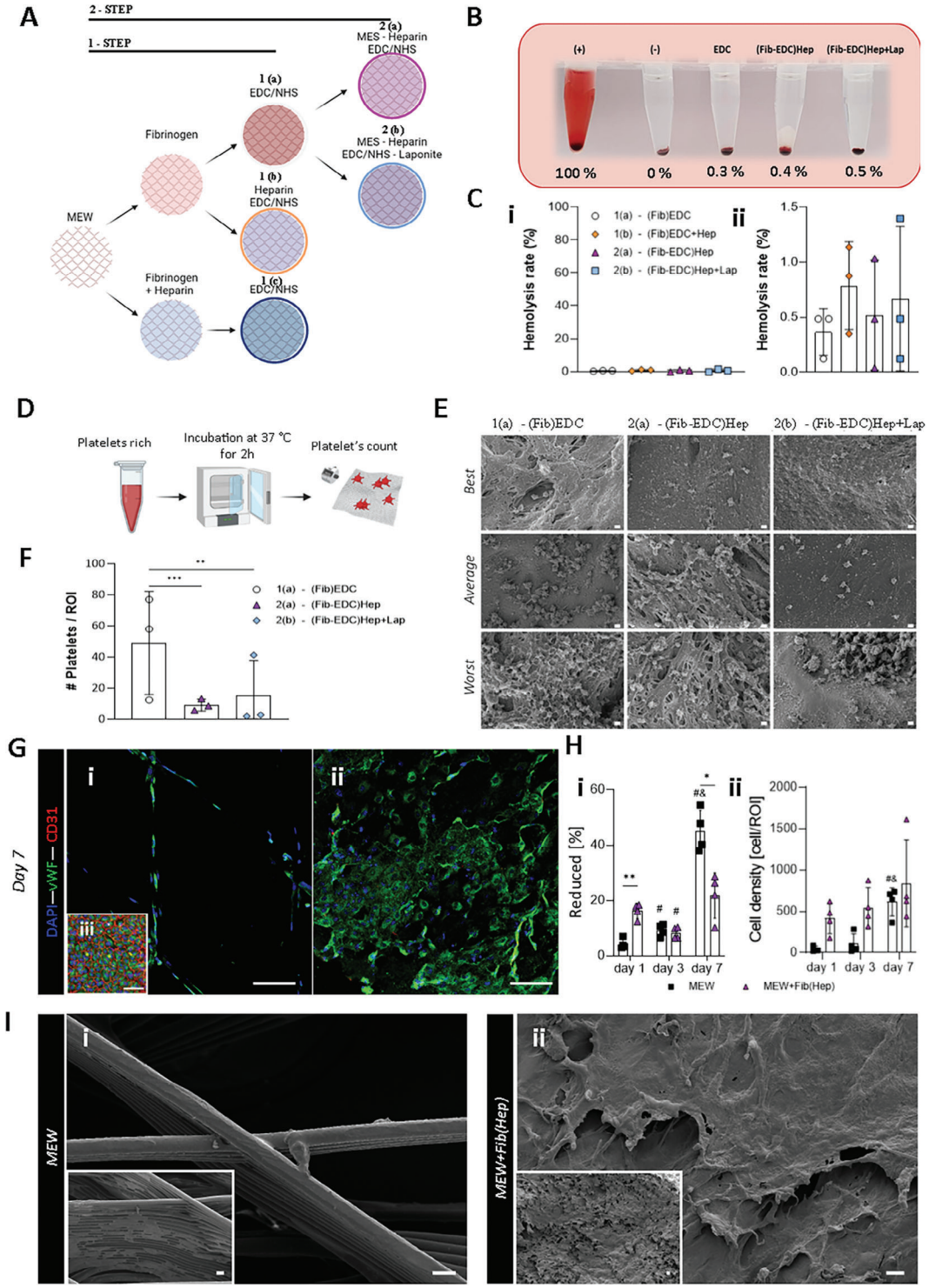

Figure 4. Effect of heparin on hemocompatibility and endothelialization. A) Schematic representation of different crosslinking methods tested to evaluate the best performing approach to bind heparin to the fibrinogen ECM. B) Qualitative images of the hemolytic assay where after incubation samples were spun down before the supernatant was collected and absorbance calculated. C) (i) Hemolysis rate for the different groups with (ii) a zoom in section to identify sample differences. D) Schematic representation of platelet adhesion assay. E) Representative SEM images of platelet rich plasma treated scaffolds. Scale bar 2 µm. F) Quantification of platelets adherent to the scaffolds after 2 h at 37 °C. ($N = 3$, $n = 10$). p value $^{*} \leq 0.05$, $^{**} \leq 0.005$, $^{***} \leq 0.001$, and $^{****} \leq 0.0001$. G) DAPI, f-actin, and CD31 staining at day 7 for (i) MEW samples and (ii) MEW+Fib(Hep), and (iii) glass slide control. Scale bar 100 µm. H) (i) AlamarBlue values of reduced percentage over time. (ii) Nuclei counting over ROI for different time points. Data showed as Mean ± SD. p value $^{*} \leq 0.05$, $^{**} \leq 0.005$, $^{***} \leq 0.001$, and $^{****} \leq 0.0001$. Evaluation of single group evolution at different time points identified by # statistically different from day 1, & statistically different from day 3. I) SEM images at day 7 for (i) MEW samples and (ii) MEW+Fib(Hep). Scale bar 20 µm.

seeded onto 8 mm diameter MEW and MEW+Fib(Hep) grafts or onto glass slides as a control and cultured for up to 7 days. DAPI, CD31, and vWf staining was utilized to assess endothelial cell behavior and the establishment of an endothelium at 3 (Figure S5C, Supporting Information) and 7 days (Figure 4G). In the MEW alone scaffolds, a number of HUVECs adhered to the PCL fibers and took on an elongated morphology with positive staining for vWf (Figure 4Gi). While the HUVEC number increased with time, HUVECs were unable to form an endothelium due to the large pore structure in the MEW alone scaffold (Figure 4Gi). On the MEW+Fib(Hep) scaffolds, HUVECs adhered in greater numbers, formed a spread morphology across the surface of the scaffold, and expressed vWf to a smaller extent CD31 over time (Figure 4Gii). While not comparable to a glass slide at 7 days (Figure 4Giii), the monolayer of HUVECs on the MEW+Fib(Hep) scaffold surface is indicative that an endothelium can form on this graft.

Moreover, differences in HUVEC adherence and proliferation over time between groups were also evident using an AlamarBlue (AB) metabolic assay (Figure 4Hi). AB-reduced percentage was significantly higher on the MEW+Fib(Hep) scaffold compared to MEW alone at day 1 indicative of enhanced cell adhesion, but this difference was inverted by day 7 where HUVECs were observed by SEM on the walls of MEW alone scaffold which increases the surface enabling cell proliferation without forming an homogenous uniform layer (Figure 4Ii). The overall number of cells in each ROI was also quantified, and a positive trend indicative of cell proliferation was identified for both groups with higher values reached for the MEW+Fib(Hep) group (Figure 4Hii). SEM images further confirmed the difference of HUVEC interaction between samples (Figure 4I). Indeed, cells were attached to the fibers of PCL frames with no further colonization of the pores. On the contrary, the formation of a partial endothelium on top of MEW+Fib(Hep) scaffolds was clearly visible (Figure 4Iii).

2.4. Handling and Mechanical Evaluation

2.4.1. Graft Handling

All vascular grafts (MEW; MEW+ES(30′); and MEW+Fib (Hep)+ES(30′)), including a control electrospun alone graft (ES(30′)), demonstrated good capacity to withstand compression and recover their original shape during handling (**Figure** 5A). Regardless of sample differences in conformation and number of layers, the internal lumen was capable of complete recovery following compression. Increasing the electrospinning time to 3 h augmented the resistance needed to completely close the lumen (Figure S6A, Supporting Information). Moreover, when tested for kinking capacity, the same trend of increased resistance was replicated for all samples. While the MEW and MEW+ES(30′) grafts demonstrated excellent bending properties, the MEW+Fib(Hep)+ES(30′) graft demonstrated a reduced ability to deform to 180° (Figure 5A). However, the lumen remained open in all grafts.

2.4.2. Graft Mechanical Behavior

Aiming to solve the current limitation in the mechanical performance of vascular grafts when compared to native tissue, the mechanical behavior of the developed grafts was analyzed and compared to both the native counterparts and the MEW alone group that was used as a control (Figure 5). A ring test was performed for all the developed scaffolds and controls. Briefly, samples were cut into 3 mm wide circular sections, positioned between two pins, and pulled at a constant velocity to rupture (Figure 5B). Stress–strain curves are reported in Figure 5Ci,ii, where all grafts follow the typical J-shape curve of soft tissues. An increased stiffness in the vascular grafts was observed with an increase in the number of components of each design. MEW+Fib(Hep)+ES(30′) and MEW+ES(30′) demonstrated a close match to MEW alone curves, while ES(30′) demonstrated an increased stiffness, particularly at higher strain levels. Data extracted from stress–strain curves are reported in Figure 5D. The elastic modulus of the TOE region and the ultimate tensile stress (UTS) of MEW+ES(30′) and MEW+Fib(Hep)+ES(30′) matched that of the native porcine carotid values (Figure 5Dii–iv). Thus, the proposed graft replicated the J-shape of native tissue[7,9] and demonstrated a high resistance to rupture.

2.4.3. Graft Implantability

Before implantation as an *off-the-shelf* solution for vascular regeneration of small diameter blood vessels, each graft was evaluated in terms of implantability as set out in ISO standard 7198:2017. Permeability, compliance, burst pressure, and suture retention were assessed (**Figure 6**). Following specific prerequisites of the standard, a set-up was assembled so that a control pressure could be applied within the lumen of the graft while images and measurements could be taken (Figure 6A). Permeability values resulted in an average well below the 800 mL cm^{-2} min^{-1} limit that would dictate a mandatory preclotting of the graft,[47,48] indicating that no preliminary contact with blood needs to be performed for any of the proposed grafts. Grafts with an external layer of electrospun PLCL demonstrated a trend of reduced permeability with the time of electrospinning, where the greater the electrospinning time the lower was the recorded permeability (Figure 6B). Indeed, a permeability of ≈1 and 0.2 mL cm^{-2} min^{-1} was reported for samples electrospun for 30 min and 3 h, respectively, while 3.5 and 0.5 mL cm^{-2} min^{-1} were reported for hybrid samples with 30 min and 3 h electrospun layer (Figure 6B,C).

Compliance was also evaluated for all grafts with the same set-up. Diameter variations at different pressures were calculated from the captured video frames with ImageJ (Figure 6D). As the tunica adventitia plays an important role in the burst pressure and compliance of native vessels, two different electrospinning times were evaluated (ES(30′) and ES(3h)) corresponding to a thin and thick adventitia. Each graft demonstrated different degrees of compliance, with the three-component graft performing most similar to that of native tissue (Figure 6E). The ES alone samples were unable to accommodate deformation following pressure increases which is consistent with the poor compliance of ES alone grafts. Interestingly, the MEW+ES hybrid grafts demonstrated an excellent capacity to tune the lumen

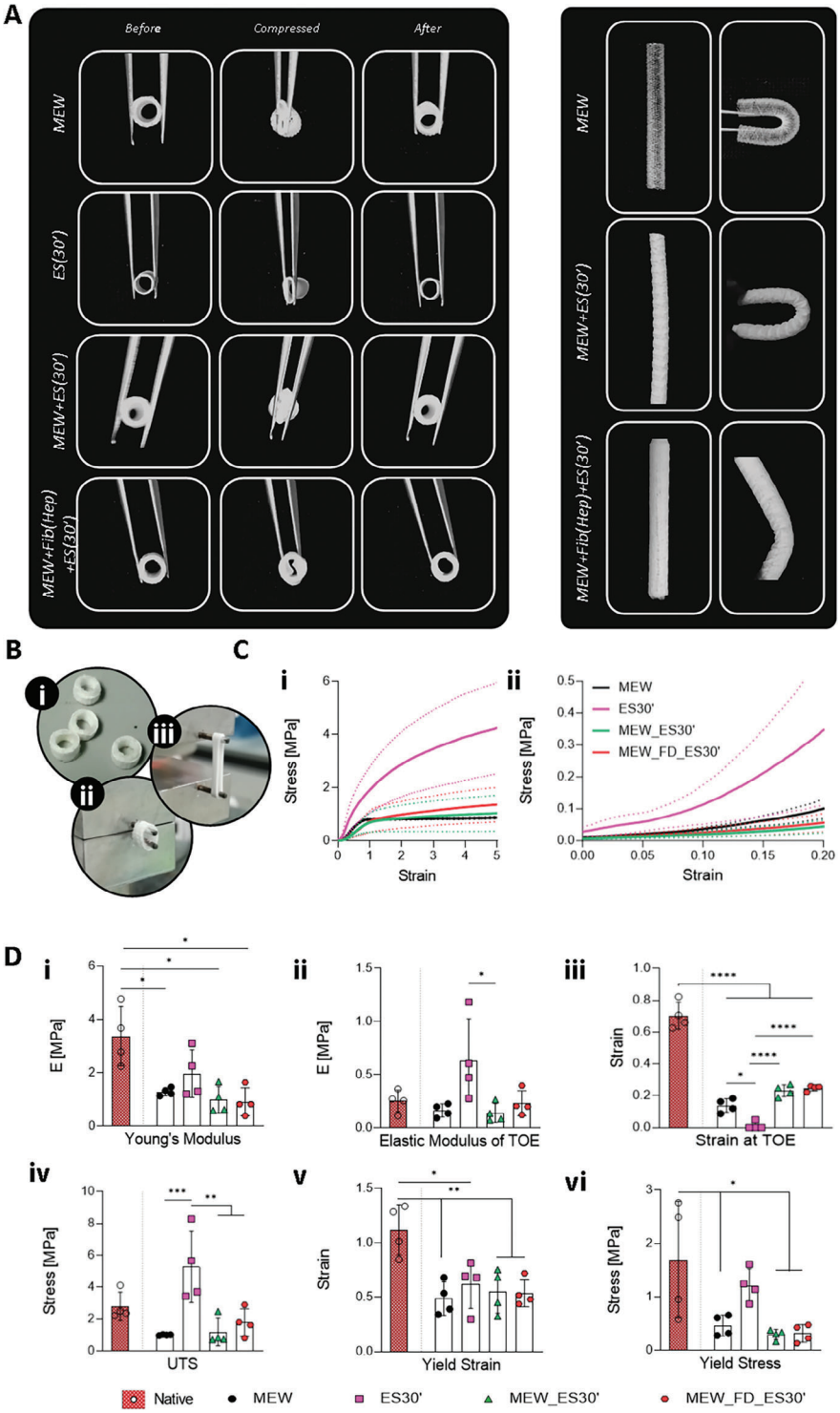

Figure 5. Handling capacity and mechanical response to ring tensile test for fabricated vascular grafts. A) Compression and recovery behavior of different grafts. From top to bottom PCL MEW frame alone (MEW), electrospun PLCL alone (ES(30′)), electrospun layer on top of PCL MEW frame (MEW+ES(30′)), and fibrinogen infused graft of PCL MEW and electrospun PLCL layer (MEW+Fib(Hep)+ES(30′)). Electrospun time was 30 min for all the groups. On the right, kinking behavior of different grafts. From top to bottom MEW, MEW+ES(30′), and MEW+Fib(Hep)+ES(30′). B) Representative images of (i) scaffold preparation and (ii-iii) testing procedure. C) Stress–strain curves obtained with ring tensile test for all grafts for 30 min of electrospinning (i) until a strain of 5 (500%) and (ii) in the physiological range of interest. D) Mechanical properties extracted from stress–strain curves. (i) Young's modulus, (ii) Elastic modulus at TOE region, (iii) Strain at TOE region, (iv) Ultimate tensile stress (UTS), (v) Yield strain and (vi) Stress. Data showed as Mean ± SD. *p* value $^{*} \leq 0.05$, $^{**} \leq 0.005$, $^{***} \leq 0.001$, and $^{****} \leq 0.0001$.

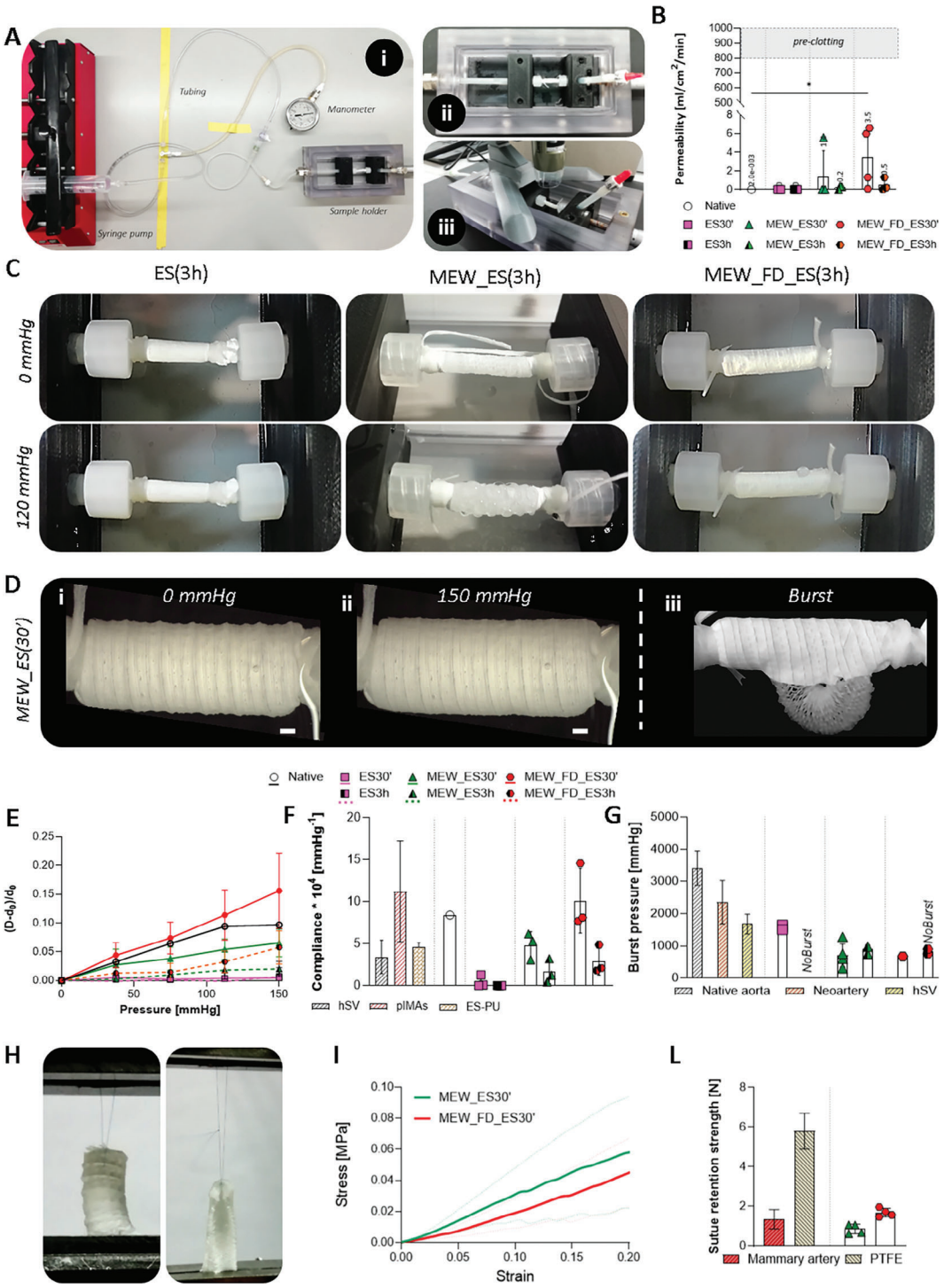

Figure 6. Vascular graft evaluation following the ISO 7198:2017 standard. A) Representation of the set-up, where a syringe pump was used to pressurize the graft with water, a series of tubing was adopted to connect the pump to the (ii) sample holder that was closed at one of the extremities after flushing the system. A manometer was used to control the pressure inside the lumen and (iii) a camera was used to evaluate variance in the diameter of the graft. B) Permeability test, quantification of water exuded through samples when pressurized at 120 mmHg over a minute. C) Representative images of samples before and after being pressurized. D) Representative images of scaffold subjected (i) to hydrostatic pressure from 0 mmHg to (ii) 150 mmHg where variation in samples diameter was recorded. Scale bar 1 mm. (iii) Representative image of a scaffold after burst occurred. E) Variation of diameter related to variation in pressure. F) Compliance data obtained between 0 and 120 mmHg of samples and literature reference[49,50] values. [hSV – human saphenous vein, pIMAs – porcine internal mammary arteries, ES-PU – electrospun polyurethan]. G) Burst values for all the samples and comparison with literature reference values.[49] [hSV – human saphenous vein]. H) Representative images of scaffold subjected to tensile stretch. I) Stress–strain curves of scaffold reaction to suture pulling test. L) Suture retention values compared to reference[47,51] values present in literature. [PTFE – polytetrafluoroethylene]. *p* value * ≤ 0.05, ** ≤ 0.005, *** ≤ 0.001, and **** ≤ 0.0001.

dimension to accommodate pressure variations. Once again, the thickness of PLCL outer layer was the leading cause of variation between hybrid samples. Interestingly, the three-component graft – MEW+Fib+ES – outperformed all developed grafts and closely mirrored that seen in native tissues (Figure 6F). The average compliance value reported for saphenous vein – in the range of 0–150 mmHg – was matched by these multicomponent grafts. In terms of compliance values, MEW+Fib(Hep)+ES(30′) reported the closest match to native vessel behavior.

Burst pressure values were recorded as the pressure at which graft integrity was lost (Figure 6G). The system adopted in this study had an upper limit of 2000 mmHg, therefore some of the grafts that demonstrated a higher resistance were not able to burst, and data were reported as nonburst (NB). ES samples were able to withstand high values of pressure before burst while MEW+ES and MEW+Fib+ES grafts demonstrated a slightly lower average with no major difference between them. Overall, a trend was visible with once again higher values reached for longer electrospinning time. Nonetheless, all tested groups reached at least 1000 mmHg, thus they are in the range of saphenous vein values (Figure 6G). Based on this analysis, MEW+ES(30′) and MEW+Fib(Hep)+ES(30′) were chosen for further evaluations.

All grafts demonstrated a capacity to be sutured, a mandatory requirement for in vivo implantation (Figure 6H). Suture pulling tests were performed with MEW+ES(30′) and MEW+Fib(Hep)+ES(30′) grafts following the requirements of the ISO 7198:2017. Suture dimensions were chosen at 8-0 in accordance with the adopted filaments for anastomosis in vivo (Figure 6H). Stress–strain curves arising from the uniaxial tensile test displayed the same trend in both grafts with a slightly stiffer response for the MEW+ES(30′) graft (Figure 6I). The ultimate force values reached were comparable to the mammary arteries values reported in the literature (Figure 6L). In conclusion, the proposed vascular grafts both exhibit suture retention strengths on par with autograft tissue, demonstrating the suitability of these grafts for implantation.

2.5. Preclinical Evaluation of Vascular Grafts

To assess the developed graft in a physiological relevant environment, an abdominal aorta substitution was performed on adult Wistar male rats. The commonly adopted eversion method failed to secure the grafts to the anastomosis of the rat abdominal aorta (AA), thus a connection device was fabricated aiming to provide a faster procedure allowing for a stable connection for both vascular grafts. This enabled an assessment of the grafts capabilities in an acute model (**Figure 7**A). MEW+ES(30′) and MEW+Fib(Hep)+ES(30′) were implanted, and both grafts demonstrated good blood flow and minimal clot formation after 1 h implantation as an abdominal aorta substitute (Figure 7A,B; Figure S7A,B, Supporting Information). Macroscopic images of harvested grafts exhibited good stability of the suture in both groups and a lumen that was free from obstructions (Figure S7A, Supporting Information). The cross section of the lumen revealed preliminary clot formation within the MEW+ES(30′) graft. Indeed, SEM images highlighted the presence of red blood cells (RBCs) and platelet accumulation on the wall of MEW+ES(30′) grafts after 1 h flow (Figure 7B). On the contrary, the MEW+Fib(Hep)+ES(30′) scaffold, demonstrated excellent hemocompatibility even after 1 h continuous blood flow, with the highly organized PCL framework still visible (Figure 7B).

A further histological analysis confirmed the difference in terms of RBCs and immune cell infiltration between the different grafts. A higher number of RBCs and nuclei was visible within the MEW+ES(30′) grafts (Figure 7C; Figure S7C, Supporting Information). The lumen was, in both cases, not impaired, and a comparable thickness of the samples was observed for the central region of the grafts. In addition, a still well-defined border was visible between the layer of MEW and ES with no delamination between the two (Figure 7C). Furthermore, the fibrinogen ECM was not damaged as a result of handling and implantation. Sections were stained for white blood cells (WBCs) to evaluate the initial immune response of the body to the grafts (Figure 7D; Figure S7D, Supporting Information), and there was an overall higher value of WBC per cm^2 for MEW+ES(30′) samples when compared to the MEW+Fib(Hep)+ES(30′) grafts (Figure S7E,F, Supporting Information), indicating the heparin-coated fibrinogen ECM dampened the initial immune response to the implants grafts.

Taken together, this data demonstrate that the MEW+Fib(Hep)+ES(30′) multicomponent vascular graft can maintain physiologically relevant blood flow and pressure while minimizing clot formation and a foreign body response, which combined with the in-vitro mechanical and biological performance, holds promise as an alternative off-the-shelf vascular graft for small diameter vessel substitution.

3. Discussion

CVD is one of the leading causes of morbidity worldwide.[1-3,6] Current treatment strategies include total vessel substitution using autologous or synthetic vascular grafts. While demonstrating good outcomes for medium and large diameter vessels, these grafts fail in small diameter applications largely due to compliance and patency mismatch to the native vessel leading to clot formation.[10-12] Therefore, in this study, we designed and developed a multicomponent vascular graft that took inspiration from native vessel architecture to overcome current challenges associated with synthetic alternatives. Building on our previously developed tubular MEW framework with vascular mimetic fiber architecture and mechanical behavior,[18] we combined this structure with a lyophilized fibrinogen matrix with tailored degradation kinetics. This hybrid construct significantly enhances cell infiltration and neotissue formation while still enabling the MEW framework to provide contact guidance controlling cell and neotissue orientation, representing the tunica media layer. This hybrid construct was further functionalized with heparin through a series of cross-linking steps, which in combination with the smooth internal ECM surface, reduced platelet adhesion and clot formation and provided a substrate for endothelization, representing the tunica intima. Lastly, an outer electrospun PLCL layer was added to the construct to improve elasticity and reduce permeability, representing the tunica adventitia. This multicomponent vascular mimetic graft satisfied ISO implantability requirements, matched the mechanical compliance of native vessels, and reestablished physiological flow with minimal clot formation in a preclinical acute rat AA substitution model. Therefore, this

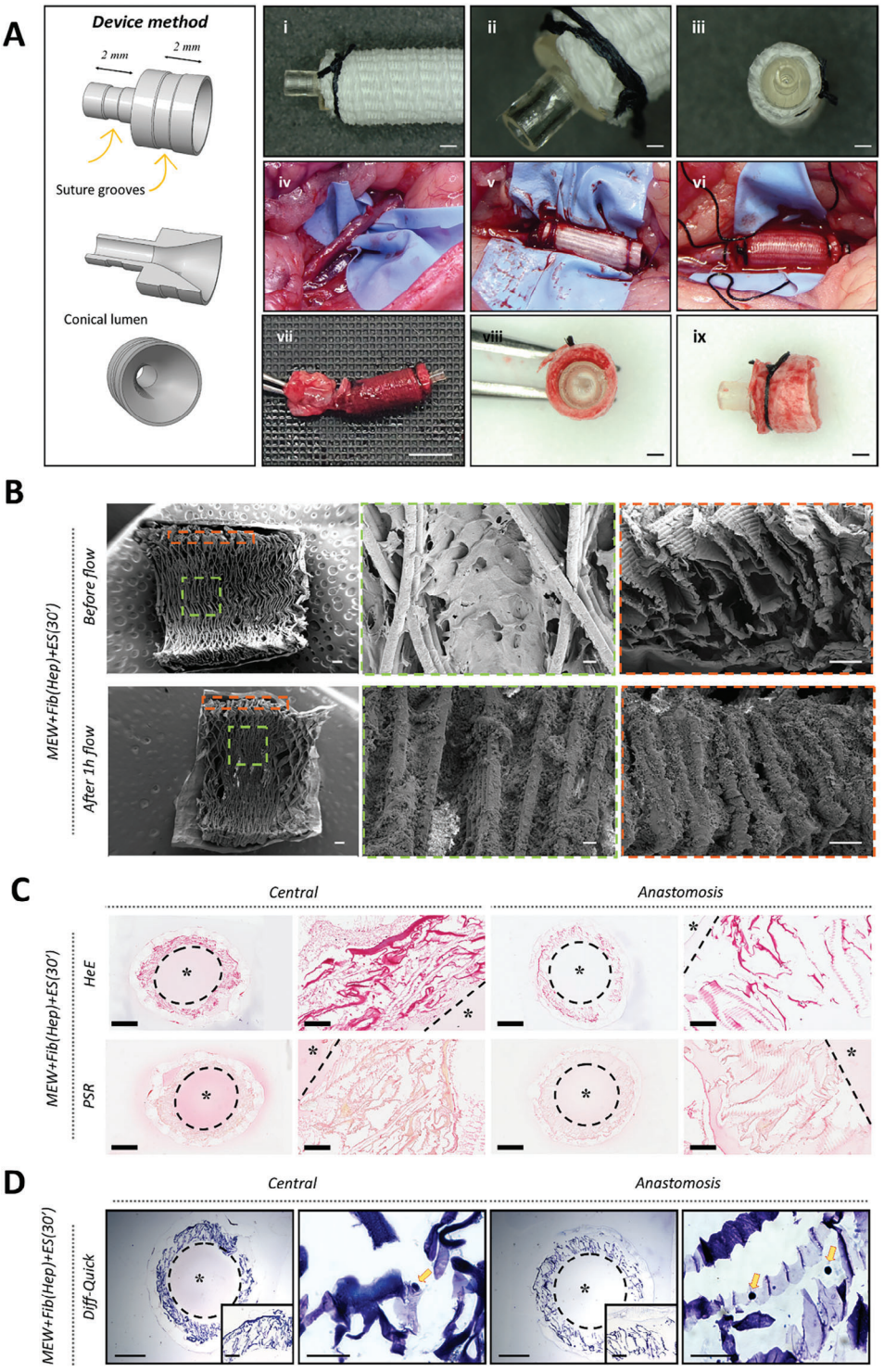

Figure 7. Vascular graft characterization following 1 h flow as a rat abdominal aorta substitute. A) Schematic CAD model of the device used to perform anastomosis of a vascular graft to a rat abdominal aorta (A.A.). (i) Stereomicroscope image of tubular graft substitute sutured to the connectors with (ii) magnification of the groove for abdominal aorta suturing and (iii) cross section. Scale bar 1 mm, 500 µm, and 1 mm, respectively. (iv) Abdominal aorta isolated from the surrounding tissues. (v) Rat A.A. connected to a tubular graft substitute before and (vi) after blood flow. (vii) Ex-vivo images of tubular vascular graft sutured by connection device method with (viii) magnification of the cross section and (vii) lateral view. Scale bar 500 µm, 1 mm, 1 mm, respectively. B) SEM images of tubular vascular graft before and after 1 h in vivo implantation as abdominal aorta substitutes. MEW+Fib(Hep)+ES(30′). Scale bar 300 µm, 20 µm, and 100 µm, respectively. C) H&E and PSR staining for MEW+Fib(Hep)+ES(30′) graft. Scale bar 1 mm, 100 µm, respectively. D) Diff-Quick staining for MEW+Fib(Hep)+ES(30′). Scale bar 100 µm, 25 µm, and 25 µm, respectively.

novel graft represents an exciting off-the-shelf alternative suitable for long-term preclinical validation and shows promise as an innovative solution to address the unmet clinical need to replace damaged small diameter blood vessels arising from CVD.

Fibrinogen-based ECM was infused within a MEW framework through an optimization of solution concentration, freeze-drying parameters, and cross-linking methods, to produce a hybrid substrate that facilitated neotissue formation and orientation in a vascular mimetic manner. Solution-based lyophilized fibrinogen scaffolds demonstrated a homogeneous pore distribution and were stabilized using either GTA or EDC/NHS. GTA is a commonly used crosslinker and fixing reagent in cardiovascular research[52,53]; however, it can be associated with toxicity, increased sample stiffness and fragility.[54] Conversely, EDC/NHS has been reported as a successful crosslinking reagent for collagen[55–60] where it maintains a stable structure at concentrations similar to that utilized here (i.e., 50 mg mL^{-1}). The pore size here reported ranged from 60 to 140 µm and closely matched the accepted range to facilitate SMC infiltration and migration,[45,46] and it is in line with previous works in the vascular field.[61] Scaffold microarchitecture – in particular its porosity and pore size – is a crucial factor in cell migration, proliferation, and ECM production[62,63] and also influences the capacity of nutrients to move throughout the construct.[64–66] As expected, the degradation rate of the fibrinogen ECM was affected by the strength of the crosslinking reagents, where GTA-treated samples remained more stable, while the EDC/NHS crosslinking resulting in a loss of more than the 50% scaffold mass after 10 days. An adequate degradation rate is a key factor to maximize tissue production and integration,[67–70] while excessively slow degradation can be a cause of chronic inflammation and potential infection, ultimately leading to graft failure.[71] The hybrid scaffolds significantly enhanced cell infiltration, ECM production, and collagen fiber deposition along preferential orientations. Despite a sharp increase in initial seeding efficiency within hybrid constructs, the infused ECM negatively impacted on cellular alignment along the major diagonal, particularly in the case of ECMs crosslinked with GTA. Thus, a relatively fast degradation rate is required to ensure the initial benefits of the ECM are maximized but to ensure the beneficial guiding properties of the PCL framework are not shielded.[18,72] This was achieved by EDC/NHS crosslinking. The presence of the fibrinogen also increased ECM production, potentially due to the rapid cell infiltration and proliferation.[67] Indeed, infilling highly porous structures with ECM components are known to enhance the scaffolds capacity to trap cells,[73] as previously confirmed with the integration of FD gelatine into 3D printed PLGA scaffolds.[74] Moreover, histological staining and polarized light analysis highlighted a preferential deposition of collagen fibers along the major diagonal for the EDC/NHS-treated scaffolds mimicking native blood vessel wall organization.[14,75] This approach to improving the bioactivity of MEW scaffolds, in combination with new materials, and significant advancements in tubular MEW technology (recently reviewed[20]) hold great promise for many tissue engineering applications. For example, by deviating from the rhombical shape to more complex auxetic designs[32,76,77] will enable further fine-tuning of mechanics for different applications across the body. Moreover, the development of more advanced multi-axis MEW printers will also facilitate the production of more anatomical accurate multi-geometrical constructs.[20,78] Taken together, the combination of an ECM component within a MEW framework significantly improves the bioactivity and regenerative properties of the MEW PCL scaffold, representing the tunica media of the multicomponent vascular graft.

To improve the hemocompatibility, heparin was bound to the hybrid graft to enhance blood interaction with reduced platelet adhesion and improved interaction with HUVECs, enabling the initial formation of an endothelial layer. The poor blood interaction and the impaired endothelialization of VGs remain among the leading causes of graft failure due to clot formation and intimal hyperplasia.[79,80] Undeniably, enhanced hemocompatibility and reduced platelet adhesion have increased vascular grafts success.[52] Heparin treatment is a common strategy to reduce platelet adhesion to scaffolds,[81,82] and is a well-known anticoagulant used clinically.[83] Through a series of optimization steps, we identified a 2-step crosslinking procedure in EDC/NHS that provided the best heparin binding, as demonstrated by the long-lasting heparin release (i.e., up to 10 days).[84] Heparin enriched scaffolds demonstrated excellent anti-hemolytic properties and significant reduction in adherent platelets both in-vitro and in-vivo. Low hemolysis is a common feature of many polymeric samples due to their low reactivity,[52,53,81] but to the best of our knowledge, no attempt has been made to implement a heparin binding approach to fibrinogen scaffolds. Moreover, when seeded with HUVECs, our hybrid constructs facilitated enhanced cell adhesion, a promising beginning to reestablish an homogeneous endothelial layer and promote homeostasis of the tissue post implantation.[80] Utilizing the infused heparin functionalized ECM as a flat substrate, EC positive staining of vWF and to a lesser degree CD31/PECAM-1 were identified after 3 and 7 days in-vitro, demonstrating the advantage to using hybrid substrates rather than a MEW-only graft. While a significant improvement in the establishment of an endothelium was identified using the hybrid constructs resulting in faint expression of CD31, further work is required to demonstrate the establishment of a fully functional endothelium on this graft. This limitation has likely arisen due to the endothelial seeding density and timeframe utilized in this study. However, these results confirmed that the internal surface architecture of the graft can be modified and chemically functionalized satisfying multiple requirements for vascular grafts, providing a platform for the initial formation of an endothelial layer, representing the tunica intima of the multicomponent vascular graft

Electrospinning PLCL onto the hybrid graft resulted in a multicomponent multilayered vascular graft that demonstrates excellent handling and implantability. Electrospinning was used to fabricate an outer homogenous layer of micron scale fibers mimicking the adventitia of blood vessels around the highly organized structure of the hybrid MEW-ECM tubular graft. PLCL is an elastic polymer that has previously been electrospun using various solvents such as hexafluoro-2-propanol (HFIP),[85] chloroform,[86] or acetic acid.[87] However, our unique solvent of formic and acetic acid was adopted as it is a less toxic solution which would improve cell viability and reduce compromising the integrity of the underlying PCL MEW framework. Together with the capacity to mimic and regenerate vascular tissues, an important aspect to consider during the development process of a vascular graft is its implantability. Sample

handling, suturability, and resistance to kinking are mandatory requirements as well as the need to remain flexible, compliant, and resistant to blood leakage.[13,88] The developed grafts also demonstrated good mechanical behavior, reproducing the typical J-shape mechanical response of native tissue under physiological relevant 10% strain range,[7,12,15] and matched the native values for elastic moduli particularly within the TOE region. The grafts also satisfied ISO 7198:2016 requirements for cardiovascular devices. Values of permeability, compliance, burst pressure, and suture retention were also tested, being among the most valuable indication of graft implantability and survival rates. With the addition of the PLCL outer electrospun layer, grafts demonstrated permeability values lower than the limit of mandatory preclotting (800 mL cm^{-2} min^{-1}),[48] thus not requiring a clotting preimplantation which would reduce surgery time. Importantly, in this work, compliance was determined to be in between the saphenous vein and the mammary artery properties which are the gold standards for autograft implantation.[49,50] Furthermore, burst pressure values obtained were close to the SV, with the longer electrospinning duration (i.e., the ES(3h) graft) giving the higher resistance, which is consistent with previous works.[47] Taken together, these findings reported the conformity of the here presented grafts to implantability requirements, overcoming the current limitations of poor mechanical properties of VG and compliance mismatch satisfying ISO standard requirements for permeability, compliance, burst pressure, and suture retention.[12,34,70,89]

The multicomponent *"off-the-shelf"* vascular graft presented herein builds on many previous approaches,[21,22,90] using FDA-approved materials and technologies, to solve the clinical need for small diameter vascular grafts. Excellent progress has been made previously in engineering vascular grafts for transplantation in-vivo. For example, L'Heureux et al. tissue-engineered a complete human blood vessel using cell-sheet technology,[19,91] while Syedain et al.[92] and Dahl et al.[93] utilized fibrin gels and PGA scaffolds respectively to engineer vascular tissue in-vitro using autologous cells which could then be decellularized as an *"off-the-shelf"* graft for implantation. All of these approaches demosntrated excellent results in-vivo largely due to biomimetic engineered tissue which possessed adequate mechancial properties and elicited a minimal immune reponse. However, each of these approaches are limited by the need for autologous cells and/or importantly the prolonged and costly manufacturng process. To overcome this, Wang and others have developed resorbable grafts consisting of electrospun polymers. While these grafts maintaing arterial pressure upon implantation they often elicited a strong inflammatory response and failed to produce sufficient neotissue within the graft.[94,95] Taking inspiration from these studies and the advancements in MEW technology, we have developed a resorbable graft which closely mirrors the mechancs of native vessels, which when combined with the heparin functionalized biological ECM provides an excellent platform to minimize inflammation and facilitae robust organized neotissue formation. Future work will focus on demonstrating the long-term potential of this graft upon implantation. The optimized step-by-step assembly sequence enables scale-up in terms of both sample production and handling, and the use of FDA approved materials and manufacturing approaches will aid in the translatability of this proposed graft.

4. Conclusion

There remains an unmet clinical need for a small diameter vascular substitution, thus an *off-the-shelf* multicomponent vascular graft was designed, fabricated, and tested to satisfy implantability requirements and successfully implanted as a vascular substitute. Three different fabrication methods and materials were used in combination to create an optimized multicomponent tubular graft enriched with heparin. The optimized step-by-step assembly sequence allowed for the scale-up in terms of both sample production and handling. This *off-the-shelf* hybrid vascular graft significantly enhanced cell yield and ECM deposition while tuning the degradation of fibrinogen further improved distribution and orientation of the engineered tissue. Moreover, heparin binding enhanced hemocompatibility while reducing platelet adhesion and supported HUVEC interaction in vitro. The adventitial inspired layer (PLCL) demonstrated decreased permeability and increased elasticity with mechanical characteristics of native vessels being matched. Thus, the proposed SDVGs were not only able to withstand physiological pressure range but also satisfied the ISO 7198:2017 requirements for medical devices – permeability, burst pressure, and suture retention. The proposed bio-inspired multicomponent vascular graft (MEW+Fib(Hep)+ES(30')) was successfully implanted as abdominal aorta substitute in a rat model and demonstrated good blood interaction with reduced infiltration of platelets and RBCs. Therefore, this novel graft represents an exciting off-the-shelf alternative suitable for long-term preclinical validation and shows promise as an innovative solution to address the unmet clinical need to replace damaged small diameter blood vessels arising from CVD.

5. Experimental Section

Vascular graft fabrication was achieved through the combination of different materials and fabrication technologies to recapitulate the specifics of each tunica. The tunica media was fabricated through the MEW of PCL, the tunica intima was integrated with lyophilized fibrinogen, while tunica adventitia was realized through electrospinning of PLCL, the specifics of which are detailed below.

Melt Electrowriting of Planar and Tubular Grafts: Briefly, as previously reported,[18] PCL was melt electrowritten to create a fibrous scaffold with defined fiber angles of 18.4°, creating a rhombus shaped pore architecture (Figure 1B). Samples were fabricated with a custom-made printer with an imposed pressure of 0.5 Bar, voltage of 6.5 kV, and a distance of 5 mm between the needle and the collector. This fibrous pore architecture was translated to a tubular format using a modified version of the MEW printer possessing a rotating mandrel collector using the following parameters: temperature of 85 °C in the barrel and 90 °C at the needle, air pressure of 0.5 bar, a voltage of 6.5 kV, and 5 mm distance between the needle and the collector.[44] The four motors were controlled by a single code so that the relationship between translational and rotating velocity was able to guarantee both a good jet profile and a specific angle orientation deposited onto the mandrel that was highly reproducible and accurate. For this study, samples with a Winding Angle (WA) of 71.6° (AR 1:3) were printed over a 3 mm diameter rod for a total number of 30 stacked layers.

Fibrinogen Infusion into MEW Grafts: MEW planar scaffolds (8 mm diameter) were treated with 2 M NaOH for 1 h at 37 °C to increase the hydrophilicity of the PCL. The samples were washed three times in PBS 1x and dried before fibrinogen infusion. A solution of fibrinogen from bovine plasma (Sigma F8630) at 50 mg mL^{-1} was injected into PDMS (PDMS, SYLGARD 184) molds containing the MEW grafts. To obtain a porous

structure, samples were freeze dried at −80 °C. To infuse the tubular MEW scaffolds with fibrinogen, a custom-made device was designed, developed, and fabricated. Briefly, a design able to place three rods with a defined thickness was drawn up and manufactured with a Form Labs 3B+ printer. PCL tubular scaffolds were first treated with NaOH 2 M for 45 min at 37 °C, washed with PBS, and positioned over the rods with O-rings on both extremities (Figure S2Bi, Supporting Information). The infusion device was then closed and tightened to prevent solution leakage. Fibrinogen solution at 50 mg mL^{-1} was slowly infused into the device from the apertures on the top leaving time and space for the air to leave the chamber. The whole device was then left at −80 °C for at least 1 h before lyophilization. A freeze-dryer Virtis Wizard 2.0 (SP scientific, Warminster, PA) was used for lyophilization. The cooling process was maintained at a rate between 0.5 and 2 °C min^{-1}, and samples were left at the specific temperature (−20°, −40° and −80°) for at least 1 h before applying the vacuum. A constant temperature of −10 °C was maintained for 18 h with an imposed vacuum pressure up to 200 mTorr to promote sublimation of ice crystals. After this phase, the temperature was raised back to 20 °C for 2 h. Once completed, samples were delicately removed from the molds and stored sealed at 4 °C until the crosslinking process.

Fibrinogen is soluble in water; therefore, all samples underwent a crosslinking step to increase the stability of the fibrinogen in an aqueous environment. An optimization of chemical crosslinkers and solvents was performed to assess scaffolds stability as well as their influence over scaffold morphology, pore size, and architecture. Samples were immersed into an ethanol solution containing carbodiimide 1-ethyl-3-(3-dimethylaminopropyl)-carbodiimide (EDC) and N-hydroxy-succinimide (NHS) weighted in a ratio of 5:2:1 with the carboxyl acid groups[96] and left for 24 h to crosslink, or alternatively in a 0.25% glutaraldehyde (GTA) solution. After three washes with PBS, the hybrid grafts were further lyophilized for better storage at 4 °C until use.

Heparin Functionalization of Fibrinogen ECM: Functionalization of heparin onto hybrid MEW+Fib scaffolds was achieved to establish an anticoagulant effect upon implantation. The crosslinking process of the fibrinogen component was modified as follows; heparin molecules were covalently attached through EDC/NHS crosslinking to the scaffolds, and different crosslinking procedures were assessed to identify the best performing approach. Three 1-step-crosslinking processes and two 2-steps-crosslinking approaches were compared in their effectiveness to bind and retain heparin. Data demonstrated that 2-step approaches gained higher yield. Briefly, hybrid grafts were first (Crosslinking1 in ethanol) crosslinked with EDC/NHS as per section, then they were immersed in a MES buffer (0.05 M) enriched with EDC, NHS, and heparin (Crosslinking2 in MES). The chosen content for EDC and NHS was optimized to a 5:2:1 ratio with the carboxyl acid groups contained in fibrinogen. Samples were left for 24 h at RT° over a shaker to react and then washed with PBS and freeze-dried.[81,82,84,97]

Electrospinning of Outer Graft Layer: Poly(L-lactide-co-E-caprolactone) (PLCL) is a co-polymer that demonstrates highly elastic behavior and improved biodegradation when compared to PCL and is thus an ideal candidate material for vascular graft fabrication. Utilizing electrospinning, a highly elastic external layer made of thin PLCL fibers could be produced covering the MEW or hybrid MEW+Fib framework. It is hypothesized that this would both increase the compliance match to that of native tissue as well as prevent any leakages from the porous MEW or MEW+Fib graft. Briefly, PLCL blocks were dissolved in a solution of formic and acetic acid in a ratio of 60:40 at different concentrations. To allow for a complete dissolution of the polymer, the solution was left stirring overnight at RT°. A 5 mL syringe with a 21G needle was inserted into a pump (Cronus Delta 2200) to impose a constant flow. The needle was positively charged, and an electric field (ΔV) applied with a high voltage apparatus (Gamma DC power supply) so that the grounded collector positioned at a specific distance (d) was able to attract fibers. The range of polymer concentrations and process parameters tested are reported in **Table 2**, with the optimal combination identified as; concentration 20%, flow rate 1 mL h^{-1}, imposed voltage 9 kV, and distance 10 cm, for a 30 min electrospinning time.

Scaffold Morphology: A bright field microscope (Olympus IX83) was used for a first preliminary assessment of precision in fiber deposition and

Table 2. Electrospinning process parameters tested for each concentration of PLCL solution.

Concentration	15%	20%	30%
Flow [mL h^{-1}]	0.5, 1, 2	0.5, 1, 2	0.5, 1, 2
$\Delta V/d$	0.9, 1.2, 1.5	0.9, 1.2, 1.5	0.9, 1.2, 1.5
d [cm]	8, 10, 12, 15	8, 10, 12, 15	8, 10, 12, 15

WA accuracy, in addition to fiber diameter. Moreover, detailed morphological characteristics were identified with a scanning electron microscopy (SEM) using a Zeiss ULTRA plus SEM with an accelerating voltage of 5 kV and with SE2 detector. Briefly, a sputter coater (Cressington 208HR) was used to deposit a gold/palladium layer on top of fibrous samples for 60 s at 40 mA. Images of the scaffolds at different magnifications were then collected.

Scaffold Porosity and Pore Size Analysis: The ethanol intrusion technique was used to determine the porosity of the constructs. Samples were weighed before and after immersion in 70% v/v ethanol solution and the total volume of ethanol was considered the empty space of the scaffold. The reported equation was used to derive the porosity of the constructs, where P_e corresponds to the porosity by ethanol intrusion, V_s the volume of the sample, d_s the density of the sample, M_s the mass of the sample, V_e the volume of ethanol, d_e the density of ethanol, and M_e the mass of ethanol.

$$Pe = \frac{Ve}{Vs + Ve} = \frac{\frac{Me}{de}}{\frac{Ms}{ds} + \frac{Me}{de}} \quad (1)$$

Quantitative evaluation of pore size was performed in an analogous manner to previous studies.[55,98] Scaffolds were snap frozen to decrease the damage during the cutting process. Cylindrical scaffolds were first cut in half in the longitudinal direction and then in half again in the transverse direction. In this way, pores were exposed in both directions, and pore size in both planes could be evaluated. Samples were embedded in 2% agarose after a hydration step in PBS 1x for 10 min. A tissue processor (Leica ASP300) was used to dehydrate the samples before wax embedding and further slicing. Each sample was sectioned at 10 µm thickness along the full height with a rotary microtome (Leica Microtome RM2235). Super frost slides were used to collect sample slices at constant intervals through the overall thickness. Slides were stained with eosin – which reacts with fibrinogen – and visualized with a Scan Scope (Aperio Technologies Inc., USA). Micrographs of every section were then captured and three digital pictures at 4x were acquired for all slides. Three samples for each condition were cut both in the longitudinal and in the transversal direction ($N = 3$) and a minimum of three slides per sample were imaged for quantification ($n = 3$). Pore size analysis was performed utilizing a custom-made MATLAB script.[55] The same process was repeated for hybrid scaffolds of MEW+Fib grafts. In this case, the analysis was performed excluding the voids left after the PCL removal with xylene. Thus, considering only the ECM structure in between the boundaries imposed by the PCL frame.

Mechanical Characterization: A ring test till failure was performed to assess the mechanical response of all grafts. Briefly, a preload of 0.01 N was applied to the scaffolds to ensure tension and correct positioning of the specimen. Samples were then stretched till failure at a rate of 10 mm min^{-1}. For each condition, four replicates were tested, and the stress–strain curves compared to that of native porcine carotid. For biological tissue (3 porcine donors), the same test was performed with a supplementary phase of preconditioning of 10 cycles up to 5% strain so that a correct realignment of collagen fibers could be obtained before testing. The following properties were determined from the resulting stress–strain curves: ultimate tensile stress (UTS), Young's modulus, yield stress and strain values, strain value of the TOE region and young's modulus of the TOE region were calculated.

Scanning Electron Microscopy (SEM): Wet samples were washed in PBS and fixed in 3% glutaraldehyde (GTA) in 0.1 M cacodylate buffer at 4 °C for a minimum of 12 h. Cacodylate buffer solution at 0.1 M was used to remove GTA residues from the samples with an incubation of 10 min repeated twice. Incubation of samples in different ethanol concentrations, 50%, 70%, 90%, and 100%, was performed to dehydrate the scaffolds. This was followed by two 30-min incubations in hexamethyldisilane (HMDS) before samples were left to dry on mounting stubs overnight to eliminate every HMDS residue. Images were acquired through scanning electron microscopy as detailed in "scaffold morphology".

Hemocompatibility Assessment: Fresh human blood was processed following previous reported protocols.[52,81] Briefly, whole blood was diluted in a 9:1 ratio with a solution of 3.8% sodium citrate. Samples were placed in 1 mL PBS 1% for 30 min before 0.02 mL of blood were added to the solution. Positive and negative controls were respectively made of dH_2O and PBS alone. The Eppendorf containing samples and blood solution were placed in the oven at 37 °C for 1 h under constant oscillation at 90 RPM. Centrifugation at 800 g for 5 min was performed to separate the particles from the aqueous phase. Absorbance values were measured at 545 nm with a spectrophotometer. Hemolysis rate was determined using the formula:

$$HR \quad (\%) = \frac{(SA - NA)}{(PA - NA)} * 100 \tag{2}$$

where SA is the absorbance of the experimental samples, and NA and PA are the absorbance of the negative and positive controls, respectively.

Platelet Adhesion: Human blood was processed without any dilution under sterile conditions. To obtain platelet rich plasma (PRP), whole blood was centrifuged at 250 g for 15 min. PRP (500 µL) was added to dry samples in a 24 well plate and positioned in an oven at 37 °C for 2 h under gently shaking. Samples were then carefully washed with PBS to eliminate all the unreacted and nonadherent blood components and fixed in 3% glutaraldehyde in 0.1 M cacodylate buffer at 4 °C for a minimum of 12 h. Scaffolds were then prepared and imaged with a scanning electron microscopy (SEM). Three samples per condition were prepared, and ten regions per scaffold were imaged and analyzed to obtain the number of adherent platelets.

Permeability and Compliance: Permeability of samples was assessed based on physiologically relevant pressure values (between 60 and 120 mmHg). The grafts were sutured onto luer fittings so that a syringe pump could be used to pressurize water within the samples. A manometer was adopted to control the pressure present inside the lumen, and a camera was used to take images of the variation in the dimension of the diameter. The volume of water that passed through the wall of the graft after 1 min of 120 mmHg internal pressure was collected and measured to evaluate permeability of samples according to the methods described in the ISO 7198:2016.[88] Permeability values for each group were calculated with the following formula:

$$\tau = \frac{Q}{A*t} \tag{3}$$

where Q is the total volume of water collected during the test, A is the area of the sample subjected to pressure (internal cylinder area by total length), and t is the testing time (min) so that permeability can be expressed as per mL×$(cm^2 \times min)^{-1}$. The obtained data were compared to native tissue as well as published data from different polymeric grafts. Moreover, with the same set-up, compliance variation for a pressure change between 0 and 150 mmHg was calculated utilizing the below formula:

$$C = \frac{(D - d_0)/d_0}{dP} * 10^4 \tag{4}$$

where D is the diameter of the sample at different pressure values between 0 and 150 mmHg, d_0 is the diameter at position zero when no pressure is applied, and dP is the variation of pressure between the two measurements.

Burst Pressure: Following the ISO 7198:2016 standard,[88] graft burst was induced with a continuous infusion of air into the lumen, while one of the two extremities of the luer fitting was closed. Briefly, air pressure was infused at incremental steps of 0.1 Bar every 10 s while scaffold deformation was recorded. Once the deformation was not following a linear pattern anymore, the pressure was not increased further, burst occurred, and the values recorded. Above 2.2 Bar the adopted system was not able to keep the pressure in the desired range. Samples that did not burst before 2.2 Bar were recorded as no-burst (NB). Nonetheless, the average value reported for saphenous vein are in the range of 2 Bar.[79]

Suture Retention Tensile Test: Strips of tubular graft of 10 mm in length and 5 mm width were prepared for each group. Following the procedure outlined in ISO 7198:2016, sutures were inserted at 2 mm distance from one extremity, and tensile grips were positioned on the opposite side.[88] The half loop created was pulled at a constant rate of 50 mm min^{-1} till failure. The strength at which the graft failed was recorded as the suture retention strength and compared to suture retention in native tissues.

Analysis of Cell and Neo-Tissue Orientation: MEW and MEW+Fib scaffolds were placed in PDMS molds and covered with fresh media consisting of Dulbecco's modified eagle's medium (DMEM, Sigma) supplemented with 10% fetal bovine serum (FBS) (Biosera lot# 11 307) and 5% penicillin and streptomycin (Sigma Aldrich) overnight for preconditioning. A concentration of 5×10^5 human bone marrow stromal cells (hMSCs) in 100 µL of media was seeded onto each scaffold. Cells were allowed to adhere for up to 6 h, and then media was topped up to reach a final volume of 500 µL. After 24 h of confinement, specimens were removed from PDMS molds and moved into a fresh well-plate where 10 ng mL^{-1} of TGFβ1 was supplemented into the growth media to stimulate differentiation. Samples were left in culture for 28 days, and media was replaced every 2 days. Live/dead images were taken using a Leica SP8 scanning confocal microscope every 7 days so that a progressive evaluation of cell viability could be performed. For the rest of the analysis – biochemical, histological, and immunostaining – samples were collected at day 1, 14, and 28.

Endothelialization Assessment: Human umbilical vein endothelial cells (HUVEC) from Lonza were cultured in EGMTM-2 Endothelial Cell Growth Medium-2 (CC-3162 Lonza) supplemented with EGM−2 SingleQuots Kit (Lonza CC-4176) containing human Epidermal Growth Factor (hEGF), Vascular Endothelial Growth Factor (VEGF), R3-Insulin-like Growth Factor-1 (R3-IGF-1), Ascorbic Acid, Hydrocortisone, human Fibroblast Growth Factor-Beta (hFGF-β), Heparin, Fetal Bovine Serum (FBS), and Gentamicin/Amphotericin-B (GA). Cells were seeded a 2500 cells cm^{-2} over collagen-coated surfaces. Briefly, a solution of 0.2 M glacial acetic acid was adopted to dilute collagen to a concentration of 0.15 mg mL^{-1}. Collagen coating was left 1 h at RT°, excess was removed, and flasks washed vigorously with PBS before any cell was seeded. HUVEC were expanded in T75 flasks at 37 °C, 95% humidity and 5% CO_2 and passaged with particular attention before 80% confluency was obtained. Cells were only centrifuged for cell counting before seeding to reduce distress and a lower velocity was used (350 g for 4 min).

A volume of 100 µL containing 5×10^5 HUVECs was seeded onto each scaffold after sterilization. After 6 h incubation at 37 °C, fresh media was added so that a final volume of 500 µL was present in each well. The day after, samples were moved to new plates and the PDMS mold removed, fresh media was replaced every second day. Metabolic activity, immunostaining, and SEM were performed at day 1, 3, and 7.

Biochemical Analysis: Samples were enzymatically digested with a papain solution with a constant rotation overnight at 60 °C. The 400 µL obtained from each sample were used to perform DNA and collagen quantification. Quant-iT Pico Green dsDNA Assay Kit (Invitrogen, P7589) was used to identify DNA content. Collagen content was identified with a further hydrolyzation of the digested solution in a 38% HCl solution for 18 h at 110 °C followed by quantification through chloramine-T assay. Hydroxyproline assay was adopted to quantify collagen content in the samples overtime: a ratio of 1:7.69 hydroxyproline:collagen, respectively[99] was used to calculate the final quantity of collagen in each sample.

Histological Analysis: At desired time points, samples were immersed and fixed in 4% paraformaldehyde. After 20 min at room temperature, samples were washed three times with PBS and embedded in a solu-

Table 3. Antibody details and dilution ratio.

Antibodies		Dilution
CD 31	AB 24590	1:200
vW- factor	AB 6994	1:200
Donkey anti-mouse 594	A 21203	1:500
Goat anti- rabbit 488	A 11008	1:500
Donkey anti-rabbit 647	AB 150075	1:200

tion of 4% agarose. This passage is mandatory for PCL samples because xylene degrades PCL fibers and agarose help to stabilize the construct and confine the tissue once the PCL frame is removed. After, dehydration and paraffin embedding, samples were sectioned at 5 µm thickness and slides collected for further staining. Overall tissue formation was assessed through Hematoxylin and Eosin (H&E), while picrosirius red (PSR) was used to stain collagen formation. Leica 5010 Auto Stainer was used to perform these stains and a Scan Scope (Aperio Technologies Inc., USA) was used to take images of the slides. Polarized light microscopy was adopted to assess collagen fiber orientation and directionality analysis.

Metabolic Activity: An AlamarBlue (AB) assay was performed to evaluate cell metabolic activity. Briefly, AB solution was diluted in EMB-2 media at a ratio of 1:9, mixed and covered from light. Samples were submerged into 400 µL AB working solution and left reacting for 2 h. The reduction values were obtained through absorbance reading at 570 and 600 nm of 100 µL in triplicates from each well. AB working solution alone was used as a blank and subtracted from each reading.

Immunohistochemistry: Samples were fixed in PFA 4% for at least 20 min at RT°. They were then washed three times in PBS and stored at 4 °C until use. Permeabilization of cell membranes was achieved with Triton X-100 0.1% (v/v) solution for 10 min and blocking of nonspecific binding sites was performed with a bovine serum albumin (BSA) solution in PBS at a concentration of 1% (w/v). Incubation of primary antibodies was performed at 4 °C overnight with dilution reported in **Table 3** for samples seeded with HUVEC. Samples were then washed in BSA 1% for 10 min and incubated, covered from light sources, for 1 h at RT° with the selected secondary at specific concentrations reported in Table 3. All samples were stained for both Phalloidin (Biosciences Alexa 488, A12379) for 20 min (1:40) and DAPI (Sigma 32670–5MG-F) for 5 min (1:2000).

Leica SP8 scanning confocal microscope was used to take images of samples at different magnification and same laser intensity. Cell alignment analysis and cell count were carried out through ImageJ plug-in directionality and cells count, respectively.

Preclinical Evaluation: The Health Products Regulatory Authority (HPRA), in exercise of the powers conferred on to it under the European Union (Protection of Animals Used for Scientific Purposes) Regulations 2012 (S.I. No. 543 of 2012) and Directive 2010/63/EU of the European Parliament and of the Council of 22 September 2010 on the protection of animals used for scientific purposes, hereby granted the project authorization number AE19136/P158 by the title of *Evaluation of New Small Diameter Vascular Grafts and Assessment of Patency Under Arterial Blood Flow Conditions*. The project was carried out and animals cared for at the Trinity Biomedical Sciences Institute, in the Comparative Medicine Unit, in Trinity College Dublin. The barrier facility research area was used to conduct all procedures under the supervision of the designated veterinary staff and surgeons.

Abdominal aorta substitution was performed on six adult Wistar male rats with a mean body weight of 500–600 g (7–9-month-old). Two separate groups were evaluated, 1) a MEW PCL tubular graft (internal ø – 3 mm) covered in an electrospun layer of PLCL (MEW_ES(30')) with an average thickness of ≈40 µm and 2) a MEW PCL tubular graft (internal ø – 3 mm) covered in an electrospun layer of PLCL with an average thickness of ≈40 µm and infused with a fibrinogen lyophilized ECM enriched with heparin (MEW+Fib(Hep)+ES(30')). Animals were sacrificed after 1 h or humanely euthanized if any distress or impairment was reported during the surgical procedure or in the hour of surveillance postsurgery.

Surgical Procedure: Rats were subcutaneously injected with pain relieving drugs (Metacam, dose 2 mg kg^{-1}) 30 min before surgery. Preoperative anesthesia was provided with 5% isoflurane and maintained ≈1.5–2.5% for the rest of the surgery. Then, the abdomen of the rat was prepared for aseptic surgery, clipped, and disinfected. A midline laparotomy incision was performed to access the site of interest. Isolation of abdominal aorta was obtained between the renal arteries and the distal bifurcation. Heparin (100 units kg^{-1}) was injected in the tail 5 min before clamping, but after aorta isolation to contain bleeding from minor vessels. Micro clamps were positioned proximally and distally on the vessel section to create a gap of ≈1.5 cm. Rat's abdominal aorta was severed, and each part flushed to remove blood clots. The rat's abdominal aorta was pierced on one side at a time and the custom-made device inserted in the opening and secured with a 5-0 silk suture. Once both sides were secured the aorta was receded and blood flow reestablished by removing the clamps. After standard control of blood flow recovery, the rats were covered and monitored for 1 h.

Vascular Graft Evaluation: Images and videos of blood flow in the distal part of the rat body were collected during the hour of the experiment. After 1 h of blood flow, grafts were excised and characterized. Macroscopic evaluation of the graft was performed with a stereomicroscope. Samples were then divided into two parts, one fixed with 4% PFA and the other fixed in 3% glutaraldehyde. The different fixation methods were adopted for tissue processing for histology and SEM, respectively.

Histological staining was performed as per previously reported protocols, samples were stained for hematoxylin and eosin (H&E) for nuclei and cytoplasm identification and picrosirius red (PSR) for collagen identification.

A diff-quick assay was also performed manually with the RAL Diff-Quik EZ-KIT kit. Briefly, samples were first deparaffined and hydrated with a Leica 5010 Auto Stainer, then manually immersed in a solution of Eosin Y 5x times followed by 7x times in a buffered solution composed of methylene blue and Azure A. Slides were washed in water and the staining stopped in alcohol. Red blood cells (RBCs), platelets, and white blood cells (WBCs) are stained differently thanks to their specific structure. Briefly, RBCs are stained in pink, platelets in violet and characterized by smaller size, while WBCs are identified with dark blue nuclei and different cytoplasm and granules color. In detail, neutrophils present with pink cytoplasm and red granules, eosinophils blue cytoplasm and red granules, and basophils have only violet granules. Interestingly, monocytes can also be identified by a violet nuclei and light blue cytoplasm. Stable samples in xylene were fixed in DPX and images were acquired with an Olympus microscope (BX41TF) at different magnifications.

Statistical Analysis: All data were analyzed and plotted with GraphPad Prism 8 (GraphPad Software, USA). One-way ANOVA test was performed and where possible Dunnett's multiple comparison was adopted. Results are reported as mean and ± standard deviation unless otherwise stated.

Ethics Approval: The Health Products Regulatory Authority (HPRA), in exercise of the powers conferred on to it under the European Union (Protection of Animals Used for Scientific Purposes) Regulations 2012 (S.I. No. 543 of 2012) and Directive 2010/63/EU of the European Parliament and of the Council of 22 September 2010 on the protection of animals used for scientific purposes, hereby granted the project authorization number AE19136/P158 by the title of *Evaluation of New Small Diameter Vascular Grafts and Assessment of Patency Under Arterial Blood Flow Conditions*.

Supporting Information

Supporting Information is available from the Wiley Online Library or from the author.

Acknowledgements

This work was supported with by the Science Foundation Ireland (SFI) under [grant number 12/RC/2278 and 17/SP/4721] and co-funded by the European Regional Development Fund and SFI under Ireland's European Structural and Investment Fund. This research has been co-funded by Johnson & Johnson 3D Printing Innovation & Customer Solutions, Johnson & Johnson Services Inc.

Open access funding provided by IReL.

Conflict of Interest

Angelica Federici reports financial support was provided by Johnson & Johnson Services Inc.

Data Availability Statement

The data that support the findings of this study are available on request from the corresponding author. The data are not publicly available due to privacy or ethical restrictions.

Keywords

cardiovascular disease, electrospinning, fibrinogen, Heparin, melt-electrowriting

Received: June 6, 2024
Revised: July 12, 2024
Published online:

[1] E. J. Benjamin, C. Paul Muntner, V. Chair Alvaro Alonso, F. S. Marcio Bittencourt, M. W. Clifton Callaway, F. P. April Carson, F. M. Alanna Chamberlain, A. R. Chang, M. Susan Cheng, F. R. Sandeep Das, F. N. Francesca Delling, M. Luc Djousse, M. S. Mitchell Elkind, F. F. Jane Ferguson, F. Myriam Fornage, F. Lori Chaffin Jordan, F. S. Sadiya Khan, B. M. Kissela, M. L. Kristen Knutson, T. W. Kwan, F. T. Daniel Lackland, F. T. Tené Lewis, J. H. Lichtman, F. T. Chris Longenecker, M. Shane Loop, P. L. Lutsey, F. S. Seth Martin, F. Kunihiro Matsushita, F. E. Andrew Moran, F. E. Michael Mussolino, et al., *Circulation* **2019**, *5*, 56.
[2] E. Wilkins, L. Wilson, K. Wickramasinghe, P. Bhatnagar, J. Leal, R. L.-Fernandez, R. Burns, M. Rayner, N. Townsend, *European Cardiovascular Disease Statistics*, Ed. 2017, European Heart Network, Brussels **2017**, pp. 174.
[3] C. D. Mathers, D. Loncar, *PLOS Med.* **2006**, *3*, e442.
[4] R. A. Byrne, G. W. Stone, J. Ormiston, A. Kastrati, *Lancet.* **2017**, *19*, 781.
[5] L. Bryniarski, M. Zabojszcz, K. L. Bryniarski, *Cardiol. J.* **2017**, *24*, 695.
[6] H. H. G. Song, R. T. Rumma, C. K. Ozaki, E. R. Edelman, C. S. Chen, *Cell Stem Cell* **2018**, *22*, 340.
[7] S. Pashneh-Tala, S. MacNeil, F. Claeyssens, *Tissue Eng. Part B Rev.* **2016**, *22*, 68.
[8] I. Skovrind, E. B. Harvald, H. Juul Belling, C. D. Jørgensen, J. S. Lindholt, D. C. Andersen, *Stem Cells Transl. Med.* **2019**, *8*, 671.
[9] H. S. Rapoport, J. Fish, J. Basu, J. Campbell, C. Genheimer, R. Payne, D. Jain, *Tissue Eng. Part C Methods* **2012**, *18*, 567.
[10] M. Carrabba, P. Madeddu, *Front. Bioeng. Biotechnol.* **2018**, *17*, 1.
[11] A. Hasan, A. Memic, N. Annabi, M. Hossain, A. Paul, M. R. Dokmeci, F. Dehghani, A. Khademhosseini, *Acta Materialia Inc.* **2014**, *10*, 11.
[12] D. B. Camasão, D. Mantovani, *Mater. Today Bio* **2021**, *10*, 100106.
[13] M. J. McClure, P. S. Wolfe, I. A. Rodriguez, G. L. Bowlin, *J. Drug Deliv. Sci. Technol.* **2011**, *21*, 211.
[14] G. A. Holzapfel, *J. Theor. Biol.* **2006**, *238*, 290.
[15] T. L. Akentjew, C. Terraza, C. Suazo, J. Maksimcuka, C. A. Wilkens, F. Vargas, G. Zavala, M. Ocaña, J. Enrione, C. M. García-Herrera, L. M. Valenzuela, J. J. Blaker, M. Khoury, J. P. Acevedo, *Nat. Commun.* **2019**, *10*, 3098.
[16] C. V. C. Bouten, P. Y. W. Dankers, A. Driessen-mol, S. Pedron, A. M. A. Brizard, F. P. T. Baaijens, *Adv. Drug Deliv. Rev.* **2011**, *63*, 221.
[17] X. Yu, R. Turcotte, F. Seta, Y. Zhang, *J. Royal Soc. Interface* **2018**, *15*, 0492.
[18] A. S. Federici, B. Tornifoglio, C. Lally, O. Garcia, D J. Kelly, D A. Hoey, *J. Mech. Behav. Biomed. Mater.* **2024**, *150*, 106292.
[19] N. L'Heureux, S. Paquet, R. Labbe, L. Germain, F. A. Auger, *FASEB J.* **1998**, *12*, 47.
[20] M. Bartolf-Kopp, T. Jungst, *Adv. Healthc. Mater.* **2024**, 2400426.
[21] B. H. Walpoth, H. G. L. Bowlin, D. Kong, J. I. Rotmans, P. Zilla, in *Tissue-Engineered Vascular Grafts*, Springer, USA **2020**.
[22] P. Gupta, B. B. Mandal, *Adv. Funct. Mater.* **2021**, *31*, 2100027.
[23] C. M. Brennan, K. F. Eichholz, D. A. Hoey, *Biomed. Mater.* **2019**, *14*, 065016.
[24] K. F. Eichholz, A. Federici, M. Riffault, I. Woods, O. R. Mahon, L. O'Driscoll, D A. Hoey, *Adv. Nano Biomed. Res.* **2021**, *1*, 2100037.
[25] K. F. Eichholz, F. E. Freeman, P. Pitacco, J. Nulty, D. Ahern, R. Burdis, D. C. Browe, O. Garcia, D. A. Hoey, D. J. Kelly, *Biofabrication* **2022**, *14*, 045013.
[26] K. F. Eichholz, D. A. Hoey, *Acta Biomater.* **2018**, *75*, 140.
[27] A. Dufour, X. B Gallostra, C. O'Keeffe, K. Eichholz, S. Von Euw, O. Garcia, D. J. Kelly, *Biomaterials* **2022**, *283*, 121405.
[28] X. Wu, W. Li, L. Herlah, M. Koch, H. Wang, R. Schirhagl, M K. Wlodarczyk-Biegun, *Mater. Today Bio.* **2024**, *26*, 101112.
[29] N. T. Saidy, F. Wolf, O. Bas, H. Keijdener, D. W. Hutmacher, P. Mela, E. M. De-Juan-Pardo, *Small* **2019**, *15*, 1900873.
[30] L. A. Bosworth, M. Lanaro, D. A. O'Loughlin, R. A. D'Sa, M. A. Woodruff, R. L. Williams, *Biofabrication* **2022**, *14*, 15015.
[31] I. Pennings, E. E. Haaften, T. Jungst, J. A. Bulsink, A. J. W. P. Rosenberg, J. Groll, C. V. C. Bouten, N. A. Kurniawan, A. I. P. M. Smits, D. Gawlitta, *Biofabrication* **2019**, *12*, 015009.
[32] N. C. Paxton, et al., *Mater. Design* **2020**, *193*, 108787.
[33] M. Bartolf-Kopp, et al., *Adv. Funct. Mater. n/a*, 2311797.
[34] F. Couet, et al., *Macromol. Biosci.* **2007**, *7*, 701.
[35] M. Castilho, et al., *Sci. Rep.* **2018**, *8*, 1245.
[36] O. Bas, E. M. De-Juan-Pardo, M. P. Chhaya, F. M. Wunner, J. E. Jeon, T. J. Klein, D. W. Hutmacher, *Eur. Polym. J.* **2015**, *72*, 451.
[37] G. Grossbacher, M. Bartolf-Kopp, C. Gergely, P. N. E. Bernal, S. Florczak, M. de Ruijter, N. G. Rodriguez, J. Groll, J. Malda, T. Jungst, R. Levato, *Adv. Mater.* **2023**, *35*, 2300756.
[38] A. Daghrery, J. A. Ferreira, J. Xu, N. Golafshan, D. Kaigler, S. B. Bhaduri, J. Malda, M. Castilho, M. C. Bottino, *Bioact. Mater.* **2023**, *19*, 268.
[39] M. J. Bissell, H. G. Hall, G. Parry, *J. Theor. Biol.* **1982**, *99*, 31.
[40] A. D'Amore, T. Yoshizumi, S. K. Luketich, M. T. Wolf, X. Gu, M. Cammarata, R. Hoff, S. F. Badylak, W. R. Wagner, *Biomaterials* **2016**, *107*, 1.
[41] S. Koch, T. C. Flanagan, J. S. Sachweh, F. Tanios, H. Schnoering, T. Deichmann, V. Ellä, M. Kellomäki, N. Gronloh, T. Gries, R. Tolba, T. Schmitz-rode, S. Jockenhoevel, *Biomaterials* **2010**, *31*, 4731.
[42] B. Tschoeke, T. C. Flanagan, S. Koch, M. S. Harwoko, T. Deichmann, V. Ella, J. S. Sachweh, M. Kellomaki, T. gries, T. Schmitz-Rode, S. jockenhoevel, Tissue Eng Part A**2009**, *15*, 1909.
[43] S. R. Caliari, J. A. Burdick, *Nat. Methods* **2016**, *13*, 405.
[44] K. F. Eichholz, I. Gonçalves, X. Barceló, A. S. Federici, D. A. Hoey, D. J. Kelly, *Add. Manufac.* **2022**, *58*, 102998.

[45] S. In, J. Hyun, J. Ik, S.-W. Cho, Y. Jung, W. Jun, S. Hyun, Y. Ha, Y. Moo, B.-S. Kim, C. Yong, S.-J. Kim, *Biomaterials* **2005**, *26*, 1405.
[46] J. Zeltinger, J. K. Sherwood, D. A. Graham, R. Müeller, L. G. Griffith, *Tissue Eng.* **2001**, *7*, 557.
[47] K. Madhavan, W. Bonani, E. Monnet, W. Tan, *J. Biomed. Mater. Res. B Appl. Biomater.* **2013**, *101*, 506.
[48] K. Maleckis, A. Kamenskiy, E. Z. Lichter, R. Oberley-Deegan, Y. Dzenis, J. MacTaggart, *Acta Biomater.* **2021**, *125*, 126.
[49] W. Wu, R. A. Allen, Y. Wang, *Nat. Med.* **2012**, *18*, 1148.
[50] L. Soletti, Y. Hong, J. Guan, J. J. Stankus, M. S. El-Kurdi, W. R. Wagner, D. A. Vorp, *Acta Materialia Inc.* **2010**, *6*, 110.
[51] L. Magnan, G. Labrunie, M. Fénelon, N. Dusserre, M. P. Foulc, M. Lafourcade, I. Svahn, E. Gontier, J. H. Vélez, V. T. N. McAllister, N. L'Heureux, *Acta Biomater.* **2020**, *105*, 111.
[52] X. Guo, J. Zhu, H. Zhang, Z. You, Y. Morsi, X. Mo, T. Zhu, *J. Colloid. Interface Sci.* **2019**, *539*, 351.
[53] G. Guo, L. Jin, B. Wu, H. He, F. Yang, L. Xu, Y. Lei, Y. Wang, *Acta Biomaterialia* **2021**, *119*, 89.
[54] J. E. Gough, C. A. Scotchford, S. Downes, *J. Biomed. Mater. Res.* **2002**, *61*, 121.
[55] M. Solazzo, M. G. Monaghan, *Biomater. Sci.* **2021**, *9*, 4317.
[56] C. Yang, *Bull. Mater. Sci.* **2012**, *35*, 913.
[57] E. Quinlan, A. López-Noriega, E. M. Thompson, A. Hibbitts, S. A. Cryan, F. J. O'Brien, J. Tissue Eng. Regen. Med. **2015**, *11*, 1097.
[58] L. H. H. Olde Damink, P. J. Dijkstra, M. J. A. Van Luyn, P. B. Van Wachem, P. Nieuwenhuis, J. Feijen, *Biomaterials* **1996**, *17*, 765.
[59] B. A. Harley, A. Z. Hastings, I. V. Yannas, A. Sannino, *Biomaterials* **2006**, *27*, 866.
[60] Z. Kočí, R. Sridharan, A. J. Hibbitts, S. L. Kneafsey, C. J. Kearney, F. J. O'Brien, *Adv. Biosyst.* **2020**, *4*, 1900212.
[61] L. Buttafoco, P. Engbers-Buijtenhuijs, A. A. Poot, P. J. Dijkstra, I. Vermes, J. Feijen, *Biomaterials* **2006**, *27*, 2380.
[62] J. J. Ross, R. T. Tranquillo, *Matrix Biol.* **2003**, *22*, 477.
[63] M. Lee, B. M. Wu, J. C. Y. Dunn, *J. Biomed. Mater. Res. A.* **2008**, *87*, 1010.
[64] A. G. Mikos, G. Sarakinos, M. D. Lyman, D. E. Ingber, J. P. Vacanti, R. Langer, *Biotechnol. Bioeng.* **1993**, *42*, 716.
[65] S. H. Oh, I. K. Park, J. M. Kim, J. H. Lee, *Biomaterials* **2007**, *28*, 1664.
[66] Y. Cao, G. Mitchell, A. Messina, L. Price, E. Thompson, A. Penington, W. Morrison, A. O'Connor, G. Stevens, J. Cooper-White, *Biomaterials* **2006**, *27*, 2854.
[67] M. J. Moore, R. P. Tan, N. Yang, J. Rnjak-Kovacina, S. G. Wise, *Trends Biotechnol.* **2021**, *40*, 1.
[68] H. Zhang, L. Zhou, W. Zhang, *Tissue Eng. Part B Rev.* **2014**, *20*, 492.
[69] H. J. Sung, C. Meredith, C. Johnson, Z. S. Galis, *Biomaterials.* **2004**, *25*, 5735.
[70] B. C. Isenberg, C. Williams, R. T. Tranquillo, *Circ. Res.* **2006**, *98*, 25.
[71] B. B. J. Leal, N. Wakabayashi, K. Oyama, H. Kamiya, D. I. Braghirolli, P. Pranke, *Front. Cardiovasc. Med.* **2021**, *7*, 592361.
[72] S. L. Edwards, J. S. Church, D. L. J. Alexander, S. J. Russell, E. Ingham, J. A. M. Ramshaw, J. A. Werkmeister, *Tissue Eng. Part C Methods* **2011**, *17*, 123.
[73] M. Cámara-Torres, R. Sinha, C. Mota, L. Moroni, *Acta Biomater.* **2019**, *101*, 183.
[74] Y. Dou, J. Huang, X. Xia, J. Wei, Q. Zou, Y. Zuo, J. Li, Y. Li, *J. Mater. Chem. B* **2021**, *9*, 4488.
[75] T. C. Gasser, S. Gallinetti, X. Xing, C. Forsell, J. Swedenborg, J. Roy, *Acta Biomater.* **2012**, *8*, 3091.
[76] F. Zhang, K. Cao, A. Zaeri, R. Zgeib, C. Buckley, Y. Ma, R. C. Chang, *Add. Manuf.* **2023**, *62*, 103383.
[77] A. Weekes, G. Wehr, N. Pinto, J. Jenkins, Z. Li, C. Meinert, T. J. Klein, *Biofabrication* **2023**, *16*, 015017.
[78] K. L. O'Neill, P. D. Dalton, *Small Methods* **2023**, *7*, 2201589.
[79] W. Jia, M. Li, H. Weng, G. Gu, Z. Chen, *Mater. Sci. Eng. C Mater. Biol. Appl.* **2020**, *110*, 110717.
[80] A. Cafarelli, P. Losi, A. R. Salgarella, M. C. Barsotti, I. B. Di Cioccio, I. Foffa, L. Vannozzi, P. Pingue, G. Soldani, L. Ricotti, *J. Mech. Behav. Biomed. Mater.* **2019**, *97*, 138.
[81] J. Zhu, D. Chen, J. Du, X. Chen, J. Wang, H. Zhang, S. Chen, J. Wu, T. Zhu, X. Mo, *Compos. Part B: Eng.* **2020**, *186*, 107788.
[82] O. Kaplan, T. Hierlemann, S. Krajewski, J. Kurz, M. Nevoralová, M. Houska, T. Riedel, Z. Riedelová, J. Zárubová, H. P. Wendel, E. Brynda, *J. Biomed. Mater. Res. A* **2017**, *105*, 2995.
[83] Z. Xu, Z. Feng, L. Guo, L. Ye, Z. Tong, X. Geng, C. Wang, X. Jin, X. Hui, Y. Gu, *J. Mater. Sci.: Mater. Med.* **2020**, *31*, 76.
[84] M. J. B. Wissink, R. Beernink, J. S. Pieper, A. A. Poot, G. H. M. Engbers, T. Beugeling, W. G. V. Aken, J. Feijen, *Biomaterials* **2001**, *22*, 151.
[85] P. Wu, L. Wang, W. Li, Y. Zhang, Y. Wu, D. Zhi, H. Wang, L. Wang, D. Kong, M. Zhu, *Biomaterials* **2020**, *242*, 119922.
[86] D. H. Kim, S.- j. H. Yun, G. Kang, J. Won, *J. Mater. Sci. Mater. Med.* **2016**, *27*, 60.
[87] S. Chung, N. P. Ingle, G. A. Montero, S. H. Kim, M. W. King, *Acta Biomaterialia* **2010**, *6*, 1958.
[88] BS EN ISO 7198: 2017 Cardiovascular implants and extracorporeal systems — Vascular prostheses — Tubular vascular grafts and vascular patches, **2017**, https://www.iso.org/standard/50661.html.
[89] B. Van de Voorde, B. Sensu, L. D. Vos, R. Colenbier, H. Baskan, J. Geltmeyer, L. Parmentier, L. Van Daele, R. I. Dmitriev, L. Pyl, K. De Clerck, S. Van Vlierberghe, *Eur. Poly. J.* **2022**, *165*, 111003.
[90] T. C. Rothuizen, F. F. R. Damanik, T. Lavrijsen, M. J. T. Visser, J. F. Hamming, R. A. Lalai, J. M. G. J. Duijs, A. J. van Zonneveld, I. E. Hoefer, C. A. van Blitterswijk, T. J. Rabelink, L. Moroni, J. I. Rotmans, *Biomaterials* **2016**, *75*, 82.
[91] N. L'Heureux, N. Dusserre, G. Konig, B. Victor, P. Keire, T. N. Wight, N. A. F. Chronos, A. E. Kyles, C. R. Gregory, G. Hoyt, R. C. Robbins, T. N. McAllister, *Nat. Med.* **2006**, *12*, 361.
[92] Z. Syedain, J. Reimer, M. Lahti, J. Berry, S. Johnson, R. Bianco, R. T. Tranquillo, *Nat Commun* **2016**, *7*, 12951.
[93] S. L. M. Dahl, A. P. Kypson, J. H. Lawson, J. L. Blum, J. T. Strader, Y. Li, R. J. Manson, W. E. Tente, L. DiBernardo, M. T. Hensley, R. Carter, T. P. Williams, H. L. Prichard, M. S. Dey, K. G. Begelman, L. E. Niklason, *Sci. Transl. Med.* **2011**, *3*, 68ra9.
[94] C. E. T. Stowell, X. Li, M. H. Matsunaga, C. B. Cockreham, K. M. Kelly, J. Cheetham, E. Tzeng, Y. Wang, *J. Tissue Eng. Regen. Med.* **2020**, *14*, 1673.
[95] Y.-L. Wu, J. M. Szafron, K. M. Blum, J. C. Zbinden, R. Khosravi, C. A. Best, J. W. Reinhardt, Q. Zeng, T. Yi, T. Shinoka, J. D. Humphrey, C. K. Breuer, Y. Wang, *Tissue Eng Part A* **2021**, *27*, 593.
[96] J. Shepherd, D. Bax, S. Best, R. Cameron, *Materials (Basel)* **2017**, *10*, 568.
[97] W. Wang, J. Hu, C. He, W. Nie, W. Feng, K. Qiu, X. Zhou, Y. Gao, G. Wang, *J. Biomed. Mater. Res. Part A* **2014**, *103*, 1.
[98] M. G. Haugh, C. M. Murphy, F. J. O'Brien, *Tissue Eng. Part C Methods* **2010**, *16*, 887.
[99] N. Y. Ignat'eva, N. A. Danilov, S. V. Averkiev, M. V. Obrezkova, V. V. Lunin, E. N. Sobol', *J. Anal. Chem.* **2007**, *62*, 51.